ELSEVIER

Polymer 41 (2000) 4317–4343

polymer

A phenomenological study of the hot-tool welding of thermoplastics Part 2. Unfilled and glass-filled poly(butylene terephthalate)

Vijay K. Stokes*

GE Corporate Research and Development, Engineering Mechanics Laboratory, P.O. Box 8, Schenectady, NY 12301, USA

Received 15 February 1999; received in revised form 28 August 1999; accepted 1 September 1999

Abstract

A hot-tool welding machine was used to study the weldability of unfilled and 30 wt% glass-filled poly(butylene terephthalate). For each of these materials, weld strength data are reported for two specimen thicknesses. In these experiments, the outflow in the melting phase was controlled by means of stops, the thickness of the molten film was controlled by the heating time, and the outflow during the final joining phase was also controlled by displacement stops. Strength data for butt welds are reported for a series of tests in which the hot-tool surface temperatures, the heating times and the displacement stop positions were varied, but the pressure was not. It is shown that very high weld strengths can be achieved in the unfilled material. In the filled material, weld strengths comparable to those achieved by vibration welding are shown to be achievable.

Keywords: Hot-tool welding; Unfilled and glass-filled poly(butylene terephthalate); Vibration welding

1. Introduction

Because of the increasing use of thermoplastics and thermoplastic composites in load-bearing applications, welding methods are becoming important for part cost reduction. One widely used technique is hot-tool welding, in which the surfaces to be joined are brought to the "melting temperature" by direct contact with a heated metallic tool. In some cases, such as joining of plastic pipes, the surfaces to be joined are flat, so that the tool is a hot plate. However, in many applications, such as in automotive headlamps and rear lights, doubly curved joint interfaces require complex tools that allow the hot surfaces to match the contours of the joint interface. Applicability to complex geometries is one of the major advantages of this process.

The hot-tool welding process is described in detail in Part 1 of this paper, which presents a phenomenological study of the hot-tool welding of BPA polycarbonate [1]. This process essentially has four phases, schematically shown by the pressure–time diagram in Fig. 1 [2]. In phase 1, the matching phase, the parts are brought into contact with the hot-tool, and pressure is maintained until the molten plastic begins to flow out laterally. In phase 2, the melt pressure is reduced to allow the molten film to thicken. In phase 3, the changeover phase, the part and tool are separated. In phase 4, the molten interfaces are brought together until the weld solidifies. There are two main variants of the hot-tool welding process. In welding by pressure the interfacial pressure during phases 1, 2 and 3 is accurately controlled. A shortcoming of this process is that the final part dimensions are not controlled directly. A modification of the above method, called welding by distance—the process used in the work described in this paper—uses rigid stops to control the process during phases 1, 2 and 3, and gives more consistent part dimensions. However, in addition to these two variants, computer controlled machines, in which pressure or displacement can be programmed over different phases of the welding cycle, are available [3].

Although considerable progress has been made in experimentally characterizing hot-tool welding [4–13], the underlying process physics has been analyzed in terms of highly simplified models [3,14–17]. For example, these models assume that the melt viscosity is constant during the final joining phase. Because the viscosity of a polymer melt can decrease by more than a factor of two for a 10°C increase in temperature, any realistic model for the welding process must account for this effect [18]. A more recent analysis of the hot-tool welding process [19] has shown that this temperature sensitivity has a dramatic effect on the process conditions within the molten layer. That analysis has also shown how the use of stops affects the welding process.

In principle, the hot-tool welding process can be used to

* Tel.: +1-518-387-5157; fax: +1-518-387-7006.
E-mail address: stokes@crd.ge.com (V.K. Stokes).

0032-3861/00/$ - see front matter
PII: S0032-3861(99)00626-6

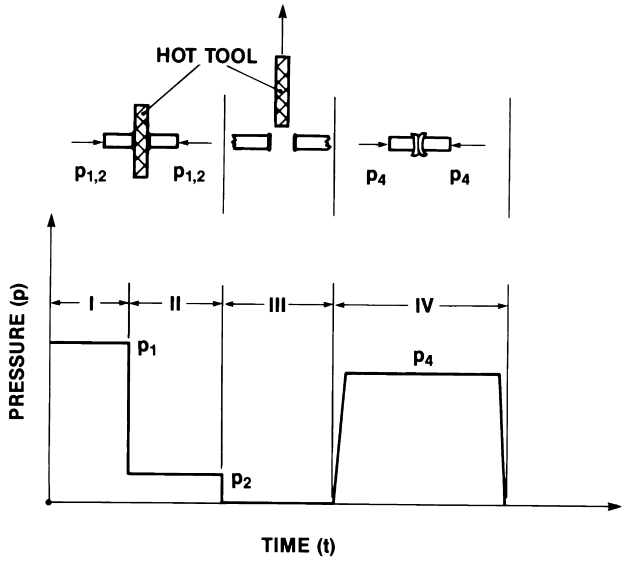

Fig. 1. Schematic pressure–time graph showing the four phases of the hot-tool welding process (adapted from Ref. [3]).

weld any polymer that melts on heating. By using different hot-tool temperatures for the two parts of an assembly, it should be possible to weld dissimilar materials [20, 21]. The literature on the welding of dissimilar materials is quite small. The few papers on hot-tool welding are mainly concerned with the weldability of different grades of HDPE [22,23], the welding of PP homopolymer to a PP copolymer [24], and the welding of polycarbonate, poly-(butylene terephthalate) (PBT), and polyetherimide to each other [25]. Certainly, the welding of dissimilar materials has not been explored systematically; nor have process models been developed.

This paper examines the hot-tool weldability of unfilled and 30 wt% glass-filled PBT. A dual platen hot-tool welding machine with displacement control, in which the temperatures of the two hot-tool surfaces can be independently controlled, was used to study the weldability of these materials. In these experiments, the outflow in the melting phase was controlled by means of stops, the thickness of the molten film was controlled by the heating time, and the outflow during the final joining phase was also controlled by displacement stops. Strength data for butt welds are reported for two specimen thicknesses for a series of tests

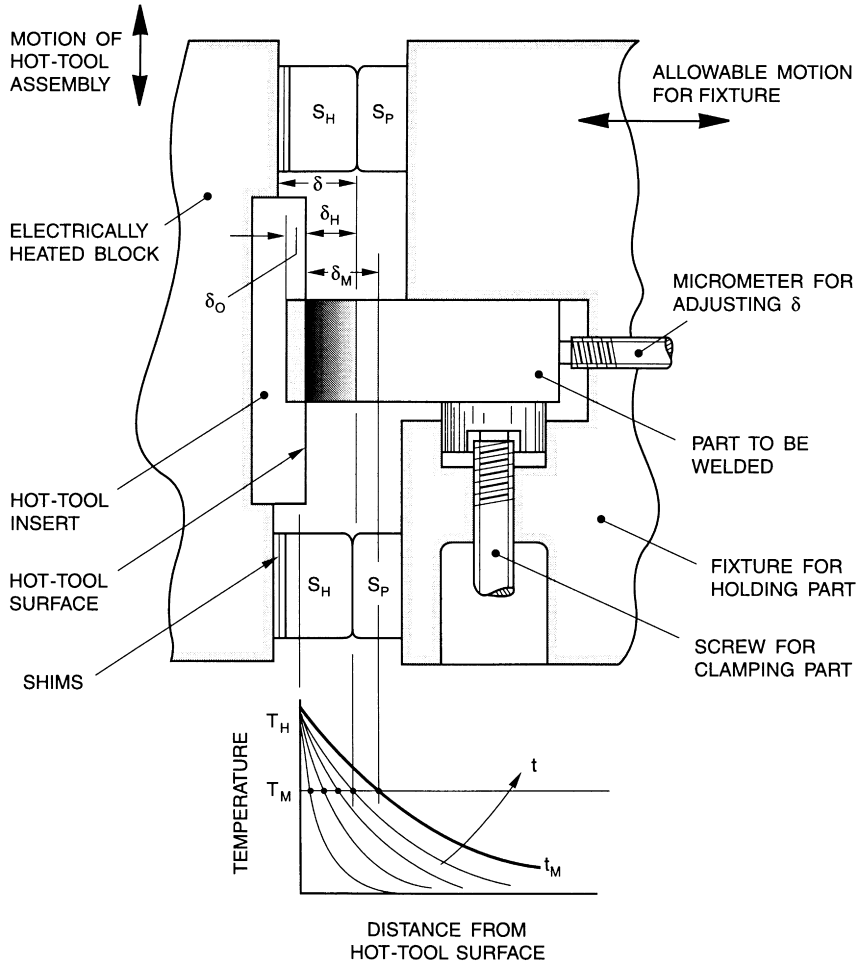

Fig. 2. Schematic diagram showing geometric parameters for displacement-controlled hot-tool welding using mechanical stops.

in which the hot-tool surface temperatures, the heating times and the displacement stop positions were varied, but the pressure was not. The effects of the large number of welding parameters were explored mainly by conducting one test per test condition studied; such data do not provide information on the variability in the weld strength at each test condition. The variability in the data were then studied through repeat tests at the near optimum conditions established by the single tests. It is shown that very high weld strengths can be achieved in unfilled PBT.

2. Displacement controlled welding

This process is described in detail in Ref. [1]. The schematic in Fig. 2 shows the essential parts of a displacement controlled welding machine, consisting of the hot-tool assembly having two exposed hot surfaces, two fixtures for holding the parts to be welded, means for bringing the parts in contact with the hot surfaces and then bringing the molten surfaces together to form the weld, and adequate timing and displacement controls. The left-hand side shows one-half of the hot-tool assembly, comprising an electrically heated block on which interchangeable hot-tool inserts can be mounted. The hot-tool assembly has mechanical stops S_H, the surfaces of which are offset from the hot-tool surface by a distance δ_H. The hot-tool assembly can be moved in and out of the configuration shown in the figure along the direction indicated.

The part to be welded is gripped in a fixture (right-hand side of figure) that can be moved to and fro in a direction at right angles to the allowable motion for the hot-tool assembly. This fixture has mechanical stops S_P that are aligned with the hot-tool stops S_H. Let the distance by which the part surface protrudes beyond the surfaces of the stops S_P be $\delta = \delta_0 + \delta_H$, as shown in the figure.

For welding, the fixture is moved to bring the part into contact with the hot-tool surface, and a pressure is applied to maintain this contact. Heat transfer raises the temperature of the part and the resulting thermal expansion causes a small rightward (away from the hot-tool surface) motion in the part and fixture. When the surface temperature reaches the melting point of the plastic, the externally applied pressure causes the molten material to flow laterally outward, thereby inducing a leftward motion of the part. The decrease in the part length caused by the outflow of molten material is called the penetration η, which for this phase is the part displacement from the instant of contact, and weld time is measured from this instant.

Initially, when the surface begins to melt, very little flow occurs and the molten film thickens. The flow or penetration rate begins to increase with time. The penetration (or part motion) will not change after the part stops S_P come into contact with the hot-tool stops S_H, as shown in Fig. 2. Let the elapsed time from the instant that the part touches the hot-tool surface to the instant when the stops come into contact be t_0, and let the corresponding penetration, the *melt penetration*, be $\eta = \delta_0$ (Fig. 2).

This thickness of material will melt and flow out laterally to form a part of the weld "bead." Continuing contact with the hot-tool surface after time t_0 will cause the molten layer to thicken with time. During this phase there will be no additional penetration. However, with increasing time, thermal expansion in the portion of the part heated by conduction will cause more material to flow out, thereby resulting in an apparent increase in δ_0. Let the duration of this film build-up phase be t_M and let the thickness of the molten layer be δ_M as shown. In the changeover phase, the parts are pulled away from the hot-tool, the hot-tool is retracted, and the molten surfaces are brought into contact—thereby initiating the joining phase. Let the duration of this changeover phase be t_c. After the molten surfaces touch, the applied joining pressure squeezes out the molten material laterally, resulting in a further penetration. During this squeezing motion, heat transfer from the melt results in a cooling and in an eventual solidification of the melt.

Two possible cases are important. If $\delta_M < \delta_H$, the part stops S_P cannot come into contact, so that part dimensions cannot be controlled. However, if $\delta_M > \delta_H$ the material in the molten layer will continue to be squeezed out until the stops S_P come into contact, after which part motion will stop and the melt will solidify without further motion. For dimensional control t_M should be large enough to ensure that $\delta_M > \delta_H$. For this case, the total penetration on each of the halves being welded will be $\delta = \delta_0 + \delta_H$, so that the overall (warm) part length will decrease by 2δ, if thermal expansion effects are neglected. Let the initial lengths of the parts before welding be l_1 and l_2, and let the length of the welded part be l_0. Then, $\Delta l = l_1 + l_2 - l_0$ is the thickness of the material that flowed out into the weld bead. If the stops come into contact during the joining phase (for which $\delta_M > \delta_H$) and thermal expansion effects are neglected, then the expected change in length should be 2δ. However, if $\delta_M < \delta_H$, then the stops will not come into contact and the change in length should be less than 2δ. Thus, if thermal expansion effects are neglected, $\Delta\eta = 2\delta - \Delta l$ is a measure for whether or not the stops come into contact: stops do and do not contact when $\Delta\eta = 0$ and $\Delta\eta > 0$, respectively. However, thermal expansion at the heated ends of the specimens would increase Δl and, in the case in which stops contact, could result in negative values of the differential penetration $\Delta\eta$. Thus, a larger Δl could result from thermal expansions both in phase 1 (an apparent increase in δ_0) and during the joining phase. Let the thermal expansion of the specimen be δ_T, so that the effective change in length would be $2(\delta + \delta_T)$. Then, $\Delta\eta_T = 2(\delta + \delta_T) - \Delta l$ will be a better measure for whether or not stops come into contact.

An estimate for this temperature-induced length increase, δ_T, is [1]

$$\delta_T = \frac{2\alpha}{\sqrt{\pi}}(T_H - T_a)\sqrt{\kappa t} \quad (1)$$

Table 1
Estimates for thermally induced length increases in PBT specimens at different hot-tool temperatures and heating times, for an ambient temperatures of $T_a = 20$°C

Hot-tool temperature (°C)	Estimate for thermally induced expansion δ_T (10^{-2} mm)		
	$t_H = 10$ s	$t_H = 15$ s	$t_H = 20$ s
215	6	7	8
230	6	7	8
245	7	8	9
260	7	8	10
275	8	9	11
290	8	10	11
305	8	10	12
320	9	11	13
335	9	11	13
350	10	12	14
365	10	13	14
380	11	13	15
395	11	14	16

in which the thermal diffusivity κ the thermal expansion coefficient α have been assumed constant (temperature independent).

This constant-property approximation requires representative values for κ and α. The density of PBT decreases continuously from 1.29 g cm^{-3} at 20°C to 1.22 g cm^{-3} at 170°C. There is a big change in the density near 203°C and it then decreases from 1.11 g cm^{-3} at 215°C to 0.99 g cm^{-3} at 380°C. The average, 1.14 g cm^{-3}, of the densities at 20 and 380°C will be used as the mean density for calculating the mean thermal diffusivity. Using a thermal conductivity of 0.28 W m^{-1} °C^{-1} and a specific heat of 1880 J kg^{-1} °C^{-1} then gives a mean thermal diffusivity of 0.13 mm^2 s^{-1}. The thermal expansion coefficient of PBT decreases continuously from 1.27×10^{-4} °C^{-1} at 20°C to 1.22×10^{-4} °C^{-1} at 140°C, and undergoes a large change near 203°C. Above 203°C, α decreases from 2.44×10^{-4} °C^{-1} at 215°C to 2.18×10^{-4} °C^{-1} at 380°C. Since the focus here is on obtaining an estimate for δ_T, an upper bound for δ_T will be obtained by using a constant thermal expansion coefficient of $\alpha = 2.3 \times 10^{-4}$ °C^{-1}, the mean of the values at 215 and 380°C. By assuming a constant κ of 0.13 mm^2 s^{-1} and a constant α of 2.3×10^{-4} °C^{-1}, the expression in Eq. (1) reduces to $\delta_T = 0.936 \times 10^{-4}(T_H - T_a)\sqrt{t}$ mm. From this expression, estimates for δ_T at different hot-tool temperatures and heating times, for an ambient temperature of $T_a = 20$°C, are listed in Table 1.

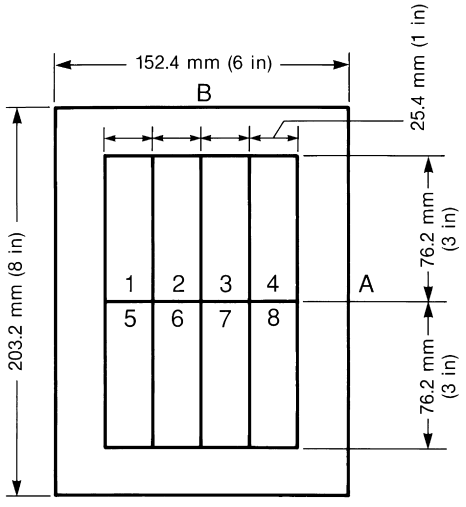

Fig. 3. Layout showing the locations of eight numbered specimens cut from 152 × 203-mm injection-molded plaques.

As the molten material cools, thermal contraction generates tensile stress in the solidifying material. This stress field can affect the residual stresses induced by the nonhomogeneous cooling. Clearly, δ_0 by itself does not contribute to the welding that occurs during the joining phase; this material just flows outward into the bead. A small value of δ_0 is required to compensate for part surface irregularities and for ensuring that contaminated surface layers flow out before the joining phase. The *weld penetration*, the penetration $\eta_j = \delta_H$ during the joining phase, is controlled by the machine setting δ_H (Fig. 1).

3. Test procedure

All the test data in this paper were obtained from 3.2- and 6.1-mm-thick specimens cut from 152 × 203-mm injection molded plaques of PBT (VALOX® 325)—which will be referred to as PBT—and from 3- and 6.1-mm-thick specimens cut from 152 × 203-mm injection molded plaques of 30 wt% glass-filled PBT (VALOX® 420)—which will be referred to as 30-GF-PBT. Eight specimens were cut from the 152 × 203-mm injection molded plaques that were gated at the 152-mm edge (gate A in Fig. 3), as per the layout shown in Fig. 3. The edges of each specimen were machined to obtain rectangular blocks of size 76.2 × 25.4 mm × thickness for assuring accurate alignment of the surfaces during butt welding along the 25.4 mm × thickness edges.

The glass-filled specimens were individually numbered according to the scheme shown in Fig. 3 [26]. Welds were conducted on sets of mating specimens from the same plaque. In this way it was possible to track variations across plaques due to fiber orientation. Fiber orientation in the specimens, which depends both on the location in the specimen as well as on its thickness, was not characterized. However, for purposes of comparison, four 152 × 25 mm specimens, corresponding to locations 1–4 in Fig. 3, were cut from the 152 × 203 mm plaques. These specimens were subjected to the same strength tests as the welded specimens, thereby providing a basis for evaluating the strengths of the welded joints.

All the welds were made on a commercially available (Hydra-Sealer Model VA-1015, Forward Technology Industries, Inc.) dual platen hot-tool welding machine in which the temperatures of the two hot-tool surfaces can be independently controlled. On this machine, the offset δ_H,

called the weld penetration, of the hot-tool stop S_H from the hot-tool surface (Fig. 2) can only be changed by inserting shims between the electrically heated hot-tool block and the stops, which are fastened to the block surface by means of screws. All the data in this paper were obtained at two weld penetrations of $\delta_H = 0.25$ and 0.66 mm. The weld specimens are pneumatically gripped in special fixtures that accurately align the specimens during the welding cycle. Each grip is provided with a micrometer that can be used to accurately set the distance δ by which each specimen protrudes beyond the stops S_P, any variations in the lengths of the specimens can easily be compensated for. In this machine, the times t_0 and t_M cannot be resolved, only the total heating time $t_H = t_0 + t_M$ can be set and measured. However, for $\delta_0 \ll \delta_H$, t_0 should be much smaller than t_M. The changeover time t_c, from the instant the heated specimens are pulled back from the hot-tool to the instant the molten films are brought back into contact, can be changed by changing the decelerating springs and the air pressure on the displacement pistons. However, the possible range of variation is quite small. In the tests reported in this paper, a fixed changeover time t_c of about 1.24 s was used; the corresponding average changeover velocity seen by the specimen molten surfaces was about 118 mm s^{-1}. The welding, or joining, time t_w, measured from the instant the molten films are brought into contact to the instant the (solidified) welded parts are released, can be preset for on this machine.

One major shortcoming of this machine is the lack of adequate pressure control at the weld interface. For 3-, 3.2- and 6.1-mm-thick welds (specimen cross-sections of thickness × 25.4 mm), the nominal weld pressures (based on the air pressure and the piston cross-sectional area) were 7.4, 6.9 and 3.6 MPa, respectively.

An important characteristic of the hot-tool surface is the extent to which molten polymer tends to stick to the surface; residue left behind can affect the quality of subsequent welds [1]. Because higher weld temperatures are required for PBT, an uncoated metal insert, made of a high-conductivity copper–nickel–silicon–chromium alloy (Ampco 940, about 96% of which is copper), was used for all the tests reported in this paper. To eliminate the effects of residues resulting from the tendency of the melt to stick to the surface, a copper scraper was used to clean the hot-tool surface after each test.

The texture of the melt surface just before the final joining phase can be expected to affect weld quality. For example, any surface roughness could trap air during the joining phase. A series of tests was done to study the effects of the hot-tool temperature and the melt time on the texture of the molten surface. 6.1-mm-thick PBT and 30-GF-PBT specimens—whose lengths had been accurately determined—were mounted in the left and right specimen holders, respectively. The micrometers were set to obtain melt penetrations of 0.13 mm on both specimens. After the specimens had been heated to the specified heating time, the specimens were retracted from the hot-tool surfaces and the weld cycle stopped. On cooling, the specimens were removed from the machine and the "heated" surfaces examined. The surfaces of the hot-tool were also examined after each test to check for residues and to determine the ease with which the hot-tool surfaces could be cleaned. Measurements of the final specimen lengths were used to determine changes in lengths. The test matrix consisted of 12 hot-tool temperatures from 230 to 395°C in steps of 15°C, and a fixed heating time of 15 s.

The test procedure for determining weld strength is described in detail in Ref. [1]. Specimens with accurately measured lengths, mounted on specimen holding fixtures with micrometer settings adjusted to obtain desired values of the overhang δ, are welded with the heating time t_H and the welding time t_w set at specified values. The length of the welded bar, having a nominal length of 152.4 mm, is accurately measured with a micrometer after sufficient cooling. The difference Δl of this final length from the combined lengths of the unwelded specimen pairs determines the thickness of the material that actually flowed out, which can be compared with 2δ. The rectangular bar is routed down to a standard ASTM D638 tensile test specimen with a butt joint at its center [26]. The tensile bar is then subjected to a constant displacement rate tensile test in which the strain across the weld is monitored with an extensometer. In this way the average failure strain across the weld over a 25.4-mm gauge length can be monitored. All the weld strength tensile tests reported in this paper were done at a nominal strain rate of 0.01 s^{-1}.

The weld flash, or "bead," was not removed in PBT specimens, and the weld strengths were obtained by dividing the load at failure by the original cross-sectional area of the specimen. Because large local deformations at the weld interface increase the local cross-sectional area, the true failure stress (based on the actual local cross-sectional area) will be smaller than the nominal stress (based on the original cross-sectional area) reported in this paper [27]. However, in some 30-GF-PBT specimens, the flash had to be sanded for the welded bar to fit in the fixture used for routing the bar down to the ASTM dogbone shape.

Furthermore, the 25.4-mm gauge length extensometer can grossly underestimate the local strain in the failure region once strain localization sets in, so that the significance of the reported failure strains ε_0 should be interpreted with care. These values only represent the lower limit of the failure strain at the weld.

Of importance are deposits on the hot-tool surfaces that could affect the temperature and surface texture seen by the specimen. Also, debris from an unclean surface could be transferred to the molten surface—the resulting contamination could affect weld strength. The hot-tool surfaces were examined and cleaned after each test. Cleaning was more difficult at higher hot-tool temperatures and longer heating times.

Table 2
Melt phase surface study of 6.1-mm-thick PBT and 30-GF-PBTspecimens. The melt time was 15 s, and the melt penetration of was 0.13 mm

Hot-tool temperature (°C)	Δl_s (10^{-2} mm)	
	PBT	30-GF-PBT
230	12	111
245	37	119
260	92	117
275	184	109
290	66	90
305	45	140
320	40	114
335	45	89
350	18	31
365	11	19
380	−13	16
395	−2	11

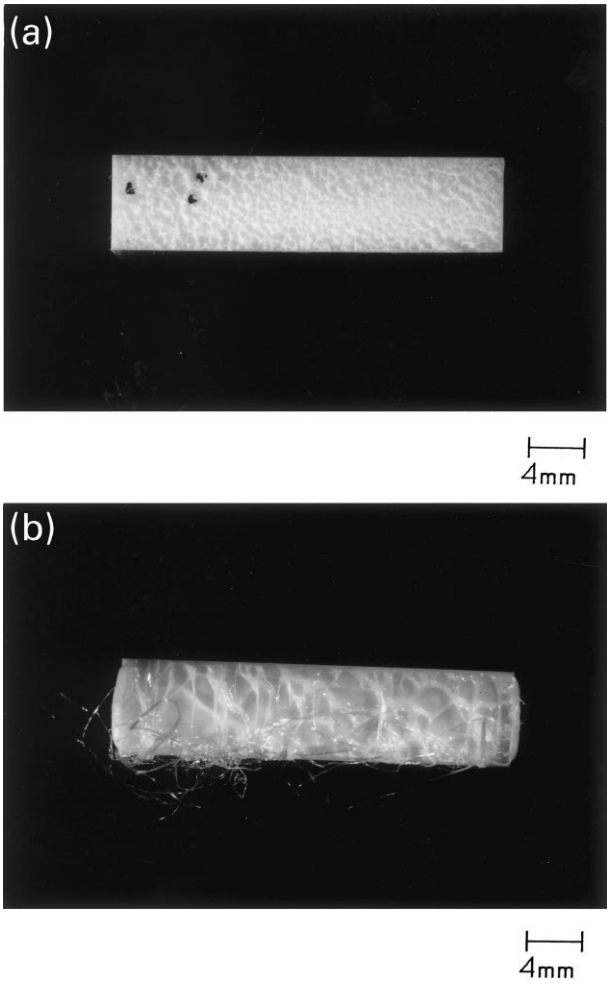

Fig. 4. Solidified molten surface textures of 6.1-mm-thick PBT specimens for a melt time of 15 s and hot-tool temperatures of (a) $T_H = 230$°C and (b) $T_H = 245$°C.

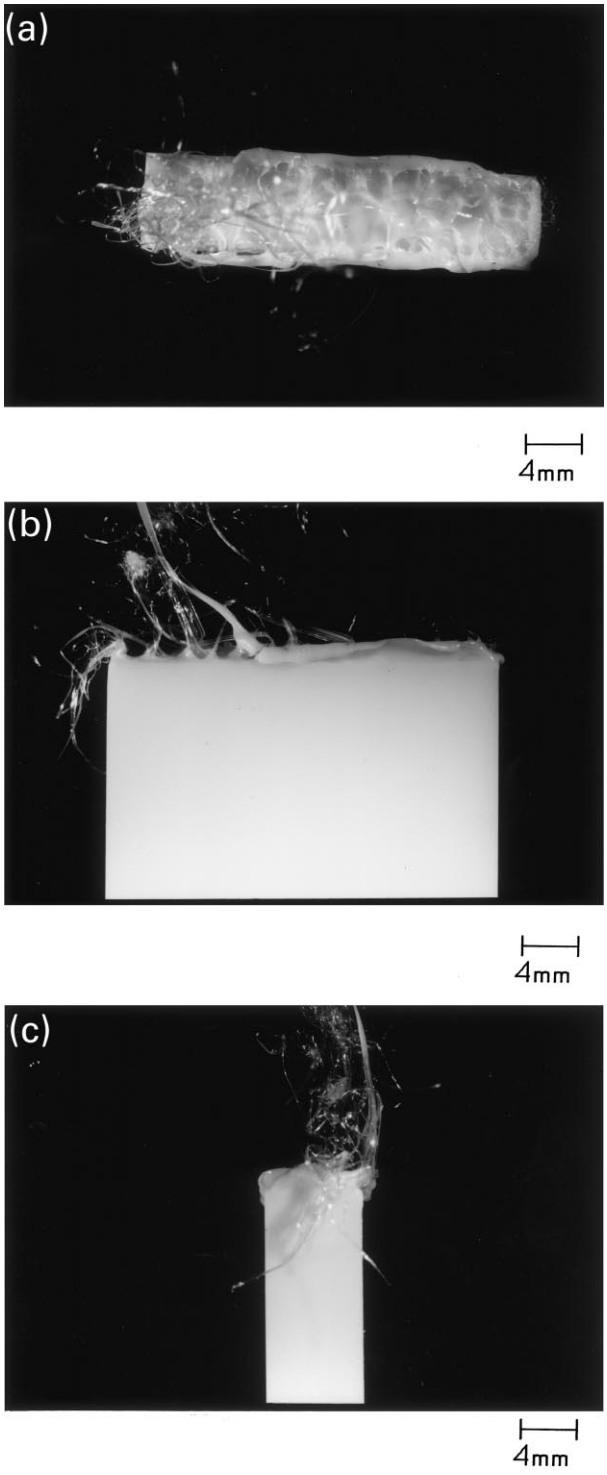

Fig. 5. (a) Solidified molten surface texture of 6.1-mm-thick PBT specimen for a melt time of 15 s and $T_H = 260$°C; (b) and (c) show the side views.

4. Molten surface texture

Air trapped between the surfaces to be joined just before the molten surfaces contact during the final joining phase can result in poor weld quality; therefore, the texture of the molten surface is important. A series of twelve tests each

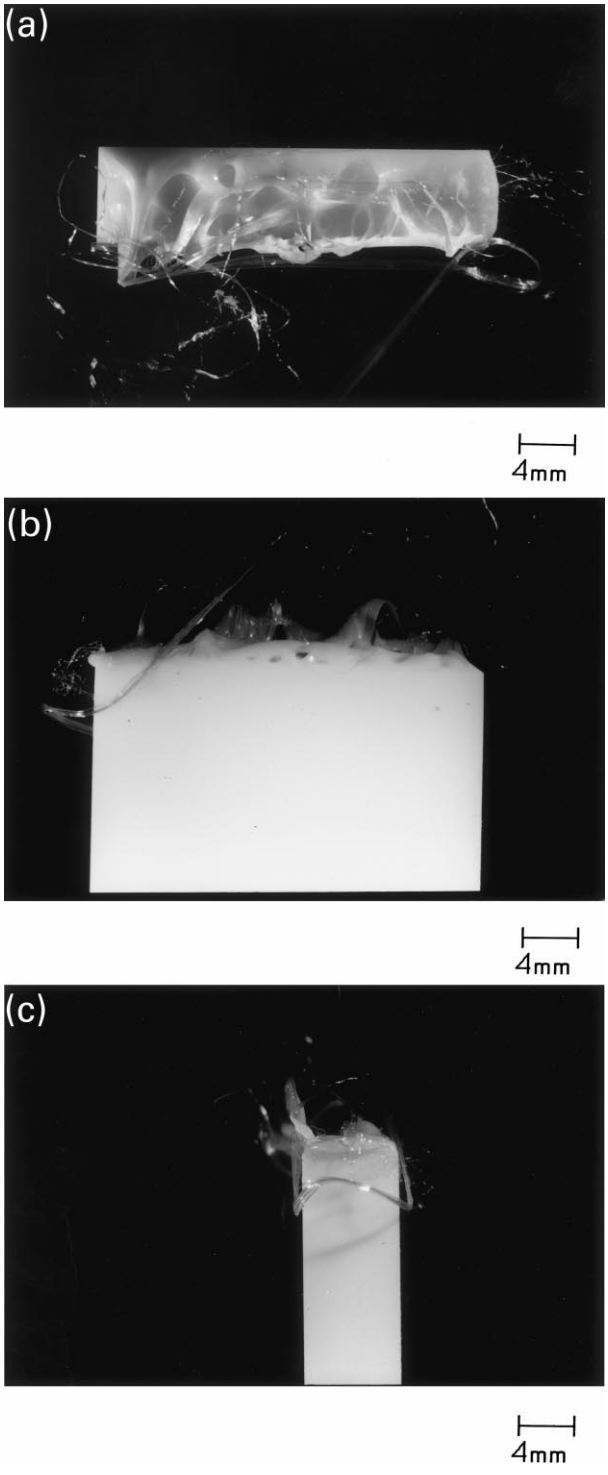

Fig. 6. (a) Solidified molten surface texture of 6.1-mm-thick PBT specimen for a melt time of 15 s and $T_H = 275°C$; (b) and (c) show the side views.

was done on 6.1-mm-thick PBT and 30-GF-PBT specimens to study the effects of the hot-tool temperature on the texture of the molten surface. For each test condition, a PBT specimen and a 30-GF-PBT specimen were heated simultaneously by using the left-hand and right-hand grips, respectively. In these tests, specimens heated to the specified heating time were retracted from the hot-tool surfaces and the weld cycle stopped. After cooling, the specimens were removed from the machine and the "heated" surfaces of the specimens examined. The surfaces of the hot-tool were also examined after each test to check for residues and to determine the ease with which the hot-tool surfaces could be cleaned. The changes in lengths of the twelve PBT and twelve 30-GF-PBT specimens, at fifteen hot-tool temperatures from 230 to 395°C in steps of 15°C, for a fixed heating time of 15 s, are listed in Table 2. With a melt penetration of 0.13 mm, the numbers in columns 2 through 9 would be expected to not exceed 13—the additional decrease in length beyond 0.13 mm resulting from thermal expansion of the heated specimen material in contact with the hot-tool.

These solidified textures for PBT, a semicrystalline resin, can be compared with those for BPA polycarbonate, an amorphous material [1]. Ref. [1] discusses a possible mechanism for "stringing" that is relevant to the discussion that follows.

4.1. Texture of PBT specimens

The textures of solidified molten surfaces were different at different hot-tool temperatures. At some temperatures "stringing" occurred—as the molten surface was pulled away from the hot-tool, very fine fibers were drawn between material sticking to the hot-tool and the molten surface on the specimen. Fig. 4a and b shows the surface features of specimens for hot-tool temperatures of $T_H = 230$ and 245°C, respectively, and $t_H = 15$ s. At the lower of the two temperatures, the surface has a rough texture, with some evidence of string initiation sites [1]. The three dark spots are residues picked up from the hot-tool surface—it is because of this possibility that the hot-tool surface has to be cleaned regularly. The surface is very different at the higher temperature, and is made up of smooth flat polygonal regions demarcated by sharp ridges. Stringing can be seen, especially at the specimen edges. The stringing is much finer than that observed in PC [1].

At $T_H = 260°C$, although the surface is again made up of smooth flat polygonal regions demarcated by sharp ridges (Fig. 5a–c)—just as for $T_H = 245°C$—the material appears to adhere to the hot-tool surface, resulting in deeper ridges and large "lips" at the edges from which stringing takes place. That is, as the molten surface is pulled away from the hot-tool, the molten material adhering to the hot-tool surface at the specimen edges is first drawn out as a thin sheet that gets drawn into very fine strings as the distance from the hot-tool surface increases. Some stringing also occurs at the ridges on the main surface.

At $T_H = 275°C$, the melt appears to adhere to the hot-tool surface even more (Fig. 6a–c). Large amounts of material are drawn out at the edges into thick sheets that cause the edges to be drawn inwards. These sheets first break up into thick "pyramidal" features that further break up into fine

strings. However, the molten surface is dominated by the relatively thick pyramidal structures. The main surface is again made up of smooth flat polygonal regions demarcated by sharp ridges.

The surface texture for $T_H = 290°C$ is different (Fig. 7a–c). The texture is no longer dominated by the edges where the lips, which are the top surfaces of lateral beads formed at the edges, are short and do not break up into pyramidal structures. The interior ridges are now more prominent, with some stringing emanating from the "peaks." However, most of the (very fine) stringing occurs near the edges.

The texture at $T_H = 305°C$ (Fig. 8a–c) is different from that at 290°C (7a–c), having a much rougher surface with many ridges from which very fine stringing occurs. The

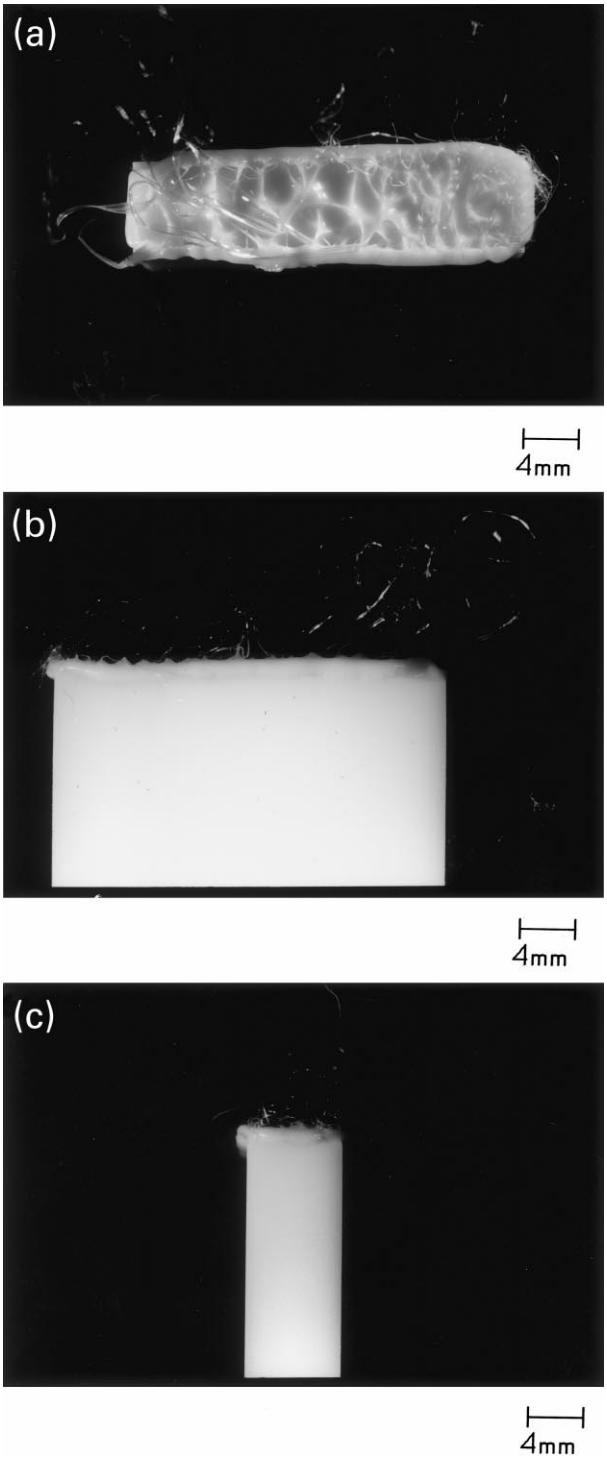

Fig. 7. (a) Solidified molten surface texture of 6.1-mm-thick PBT specimen for a melt time of 15 s and $T_H = 290°C$; (b) and (c) show the side views.

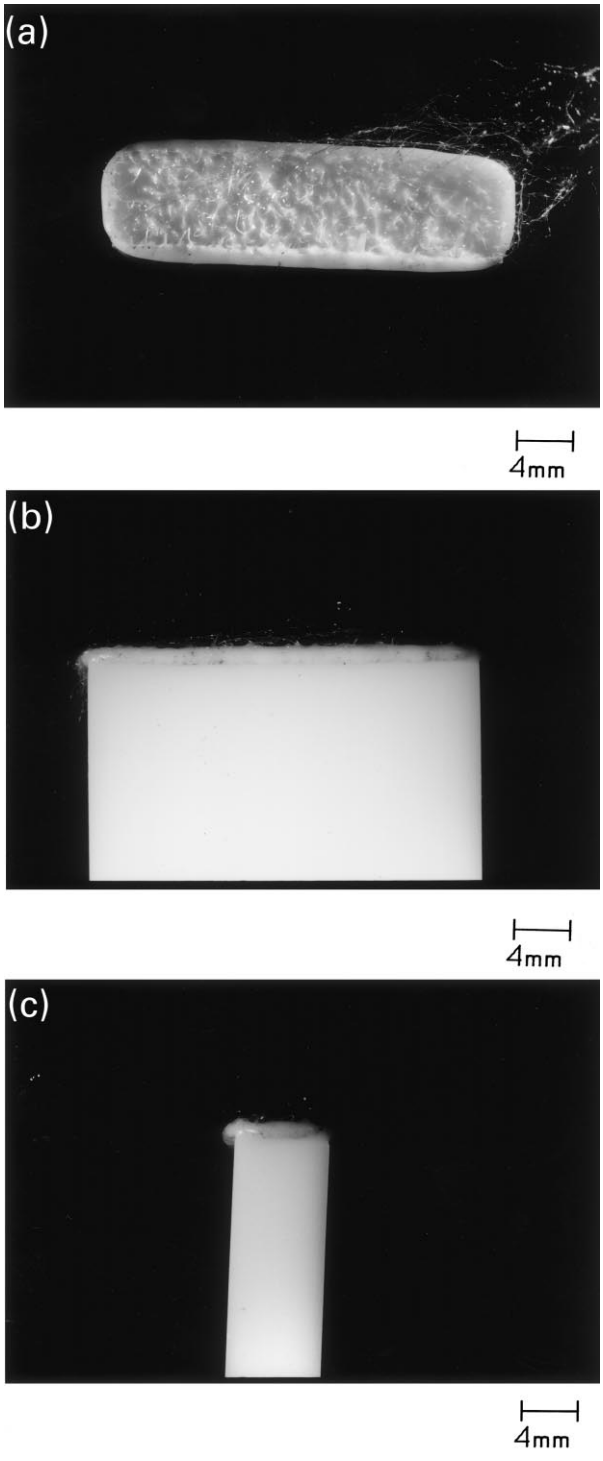

Fig. 8. (a) Solidified molten surface texture of 6.1-mm-thick PBT specimen for a melt time of 15 s and $T_H = 305°C$; (b) and (c) show the side views.

edges have pronounced lateral beads. The surface texture at 320°C is similar, but with less stringing.

At $T_H = 335$°C, the surface texture is again different (Fig. 9a–c). The surface has fewer features and the ridges are rounded rather than sharp. The edges have very pronounced lateral beads. There is almost no stringing. The texture at $T_H = 365$°C is similar.

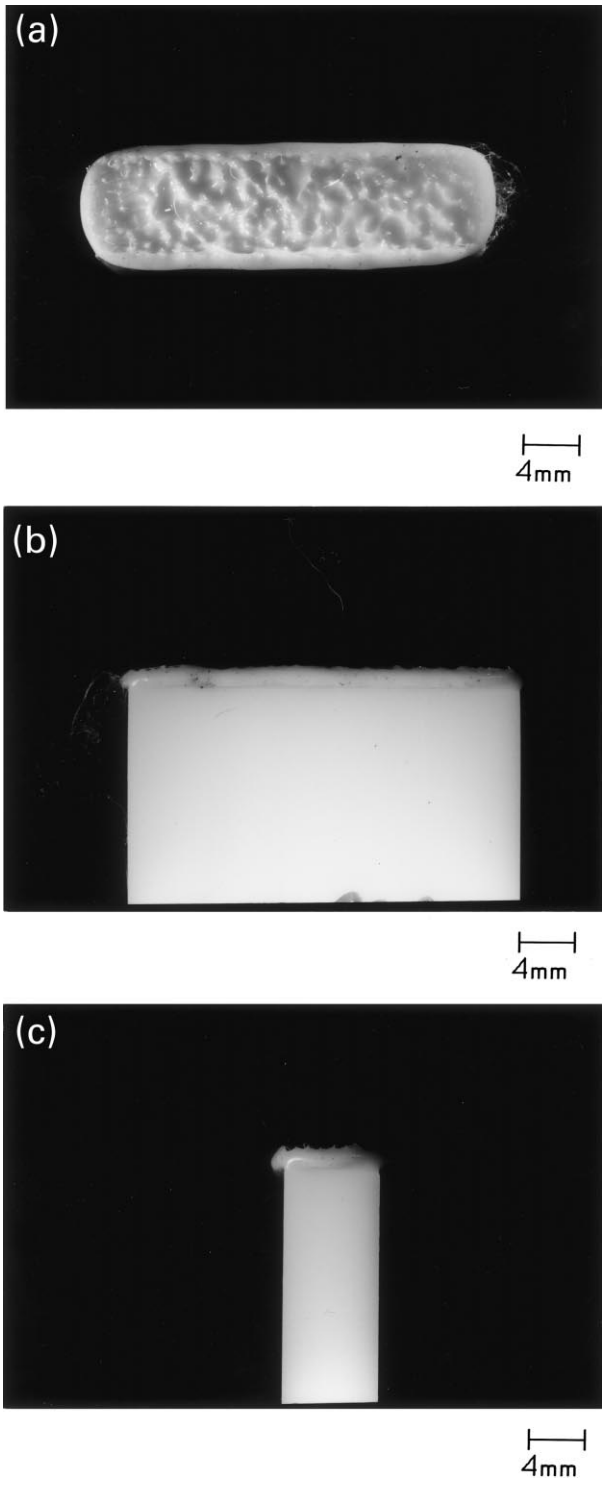

Fig. 9. (a) Solidified molten surface texture of 6.1-mm-thick PBT specimen for a melt time of 15 s and $T_H = 335$°C; (b) and (c) show the side views.

4.2. Texture of 30-GF-PBT specimens

The textures of the glass-filled PBT surfaces are different from those for the neat resin. This difference can be attributed mainly to preferential outflow of resin, leaving the interior of the surface fiber rich. Fig. 10 shows the texture for $T_H = 230$°C, which is relatively flat in comparison to that of the neat resin (Fig. 4a). This flatness can be explained by the molten resin being squeezed out to form very thin lips that are not present in the neat resin surface. The black specks are residues picked up from the hot tool; the thick gray lines are shadows cast by thin lips at the edges. The surface textures for $T_H = 245$°C is similar, except that strings form in the lip. At $T_H = 260$°C, pronounced outward protruding lips are formed at the edges.

At $T_H = 275$°C, the surface texture (Fig. 11a–c) consists of a rough "porous" interior, mainly made up of glass-fiber rich regions, from which the resin has flowed into lips at the edges. While thin, low pyramidal structures form at the edges, there is no stringing. Because of unavailability of sufficient resin at the surface, the size of the drawn out material at the edges is much smaller than for the neat resin (Fig. 6a).

The surface texture for $T_H = 290$°C (Fig. 12a) exhibits evidence of "pitting." This pitting, or porosity increases at $T_H = 305$°C (Fig. 12b). The surface texture at $T_H = 320$°C is similar to that at 305°C. At $T_H = 335$°C, the surface texture exhibits even more pitting (Fig. 12c)—similar behavior with resin-rich edges is observed at $T_H = 350$, 365, 380 and 395°C.

As mentioned earlier, with a melt penetration of 0.13 mm, the decreases in the lengths of specimens, Δl_s, listed in Table 2, should not exceed 13—the additional decrease beyond 0.13 mm resulting from thermal expansion of the

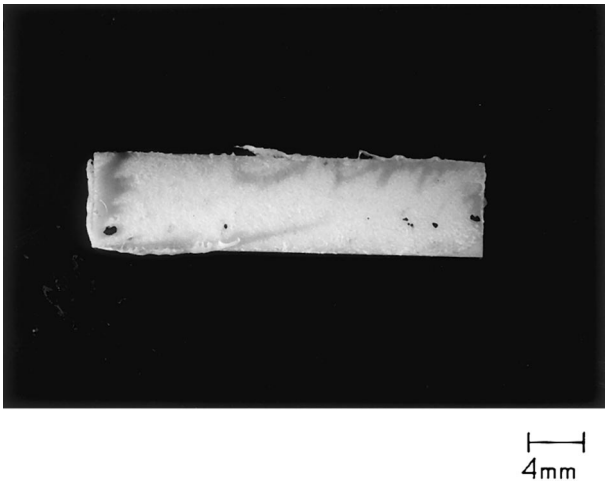

Fig. 10. Solidified molten surface textures of 6.1-mm-thick 30-GF-PBT specimens for a melt time of 15 s and a hot-tool temperatures of $T_H = 230$°C.

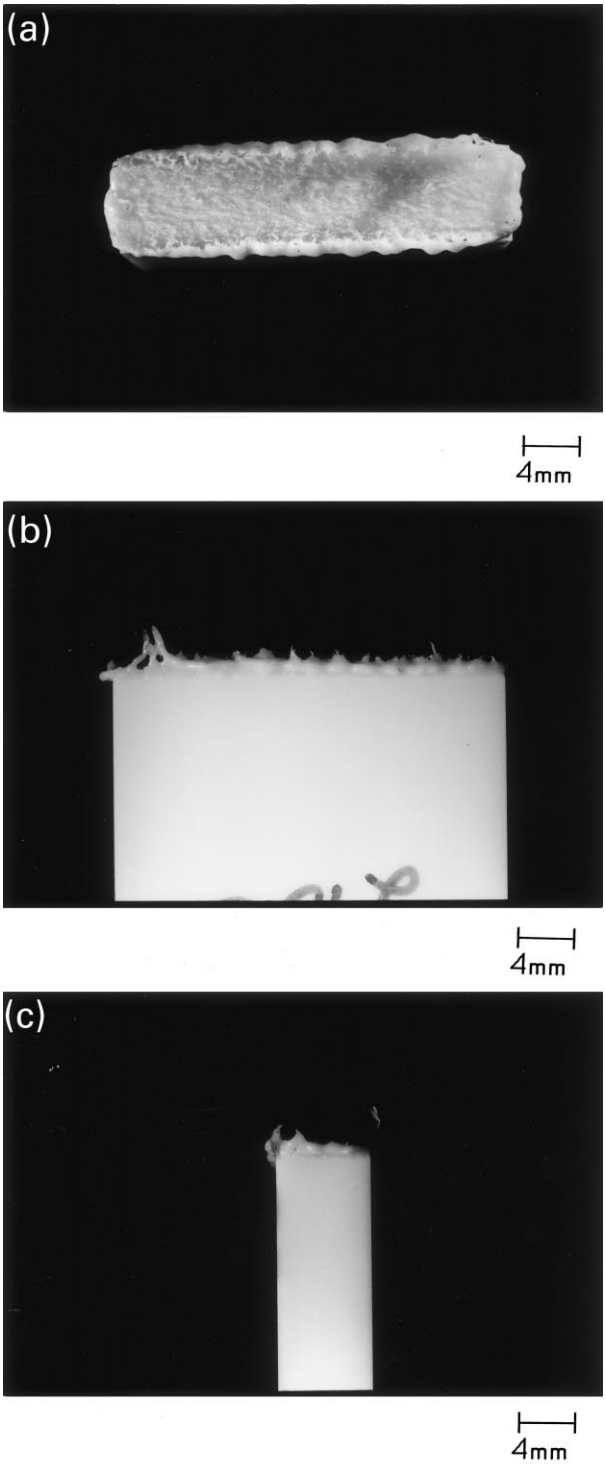

Fig. 11. (a) Solidified molten surface texture of 6.1-mm-thick 30-GF-PBT specimen for a melt time of 15 s and $T_H = 275°C$; (b) and (c) show the side views.

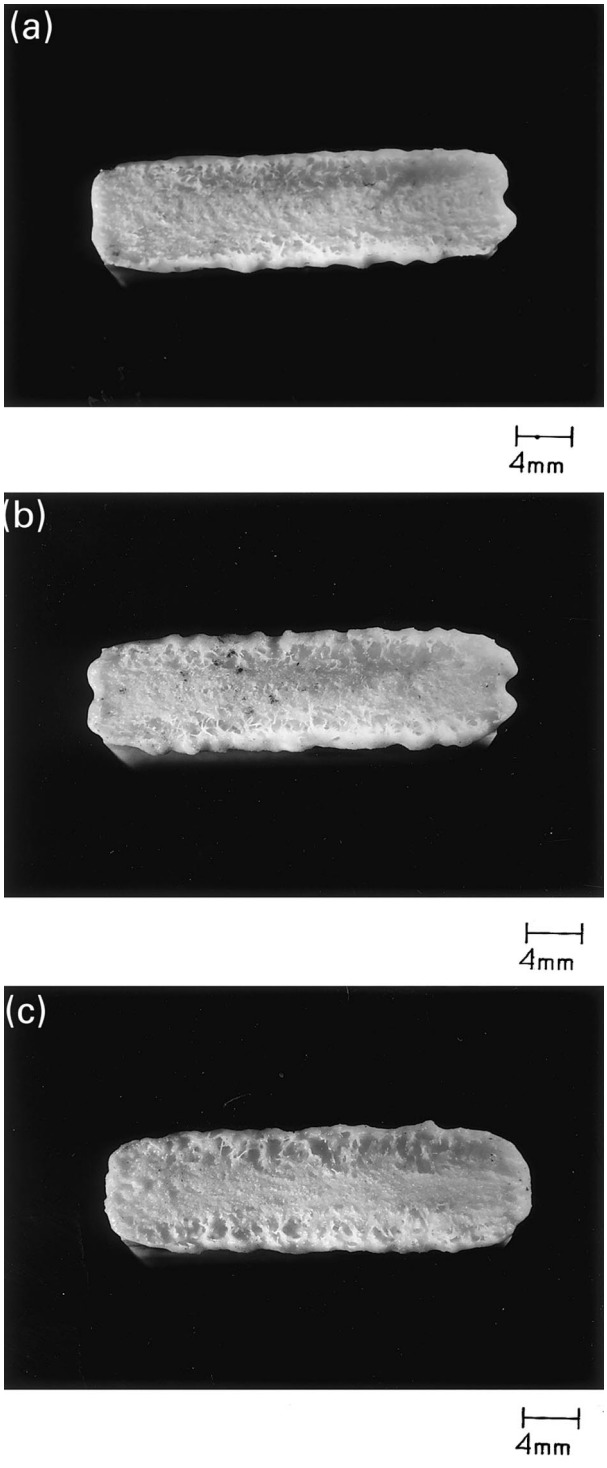

Fig. 12. Solidified molten surface textures of 6.1-mm-thick 30-GF-PBT specimens for a melt time of 15 s and hot-tool temperatures of (a) $T_H = 290°C$, (b) $T_H = 305°C$, and (c) $T_H = 335°C$.

heated specimen material in contact with the hot-tool. The data in this table show that, except in a few cases, Δl_s is larger than 0.13 mm. Values of Δl_s smaller than 0.13 mm, including negative values, imply an increase in the specimen lengths. The values of Δl_s decrease systematically at higher temperatures, both for PBT and 30-GF-PBT. This is consistent with the tendency of the material to stick to the hot-tool surface at higher temperatures, causing the molten/softened material to neck and draw, thereby resulting in an apparent increase in the specimen length. In general, the

Table 3
Strength and ductility data for hot-tool welds of 3.2-mm-thick PBT specimens, at a strain rate of $\dot{\varepsilon} = 0.01\ s^{-1}$, as functions of the hot-tool temperature and the heating time, for two weld penetrations of 0.25 and 0.66 mm. The melt penetration was maintained at 0.13 mm, and the seal time was kept constant at 10 s

Hot-tool temperature (°C)	Heating time (s)	Weld strength[a] (MPa)		Failure strain[b] (%)		Δl (mm)		Differential penetration $\Delta\eta$ ($\Delta\eta_T$) (10^{-2} mm)	
		$\delta_H = 0.25$ mm	$\delta_H = 0.66$ mm	$\delta_H = 0.25$ mm	$\delta_H = 0.66$ mm	$\delta_H = 0.25$ mm	$\delta_H = 0.66$ mm	$\delta_H = 0.25$ mm	$\delta_H = 0.66$ mm
230	10	19.7	17.3[c]	0.83	0.75	0.71	0.55	5 (17)	103 (115)
245	10	18.4	16.1[c]	0.77	0.63	0.90	0.83	−14 (0)	75 (89)
260	10	18.1	25.6[c]	0.73	1.05	1.02	1.19	−26 (−12)	38 (52)
275	10	53.5	35.1	3.01	1.44	1.09	1.35	−33 (−17)	23 (39)
290	10	50.4	46.6	2.63	1.98	1.16	1.56	−40 (−24)	1 (17)
305	10	56.3	56.8	4.58	2.69	1.24	1.69	−48 (−32)	−11 (5)
320	10	50.7	55.4[c]	3.15	2.93	1.17	1.80	−41 (−23)	−23 (−5)
335	10	49.8	58.3	3.01	3.49	1.31	1.89	−55 (−37)	−32 (−14)
350	10	–	57.5	–	3.74	–	1.84	–	−27 (−7)
365	10	–	59.9	–	3.74	–	1.96	–	−38 (−18)
380	10	–	42.8	–	–	–	2.07	–	−50 (−28)
230	15	20.1	10.2[c]	–	0.42	0.73	0.64	3 (17)	94 (108)
245	15	39.9	21.5	1.94	0.83	1.10	1.02	−34 (−18)	56 (72)
260	15	50.5	32.0	2.79	1.25	1.05	1.36	−29 (−13)	22 (38)
275	15	52.0	47.0	2.79	2.10	1.13	1.49	−37 (−19)	9 (27)
290	15	53.8	48.1	3.55	2.12	1.21	1.70	−45 (−25)	−13 (7)
305	15	53.2	59.1	3.45	3.15	1.22	1.88	−46 (−26)	−30 (−10)
320	15	48.0	59.1	–	3.96	1.27	1.97	−51 (−29)	−39 (−17)
335	15	43.6	54.3[c]	2.31	2.83	1.16	2.02	−40 (−18)	−44 (−22)
350	15	–	58.1[d]	–	4.27	–	1.99	–	−42 (−18)
365	15	–	43.1	–	1.86	–	2.02	–	−44 (−18)
380	15	–	26.7	–	–	–	2.01	–	−43 (−17)
230	20	12.9	12.5	0.52	0.49	0.73	0.70	3 (19)	88 (104)
245	20	42.3	23.6	2.08	0.98	1.14	1.23	−38 (−20)	34 (52)
260	20	50.4	29.2	2.80	1.20	1.07	1.23	−31 (−11)	9 (29)
275	20	50.6	51.7	2.74	2.29	1.19	1.78	−43 (−21)	−20 (2)
290	20	32.5	58.0	1.39	2.95	1.23	1.87	−47 (−25)	−29 (−7)
305	20	54.1	62.5	3.36	4.59	1.21	1.94	−45 (−21)	−37 (−13)
320	20	45.3	58.4	2.97	3.91	1.10	2.03	−34 (−8)	−46 (−26)
335	20	39.6	49.8	2.08	2.15	0.92	2.10	−16 (10)	−52 (−26)
350	20	–	57.9	–	3.25	–	2.10	–	−52 (−24)
365	20	–	40.0	–	1.73	–	2.01	–	−43 (−15)
380	20	–	[e]	–	[e]	–	[e]	–	[e]

[a] $\sigma_0 = 64.8$ MPa.
[b] $\varepsilon_0 = 3.64\%$.
[c] Specimen had debris on weld surface.
[d] Specimen yielded below the weld.
[e] Specimen did not weld.

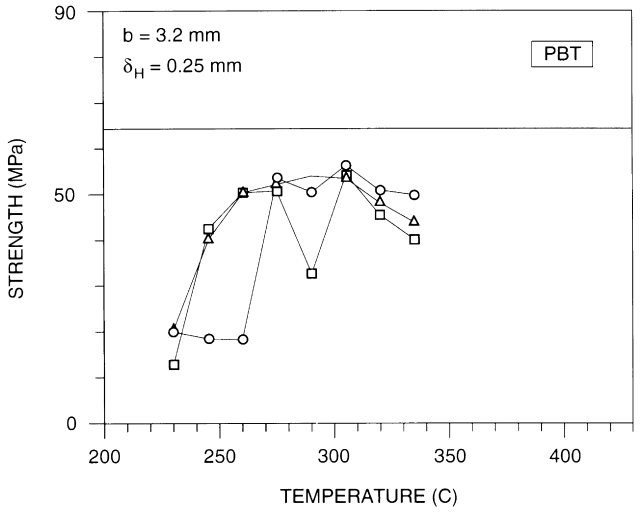

Fig. 13. Weld strength of 3.2-mm-thick PBT as a function of the hot-tool temperature, with the heating time as parameter. Circles, triangles and squares correspond, respectively, to heating times of 10, 15 and 20 s. The melt and weld penetrations were maintained at 0.13 and 0.25 mm, respectively.

reduction in the lengths of the PBT and 30-GF-PBT specimens is larger than the changes in PC specimens [1].

5. Weld strength of PBT

In this paper, the total time $t_H = t_0 + t_M \approx t_M$ for which the specimen is in contact with the hot-tool will be referred to as the heating time; melt penetration will refer to the distance δ_0 (Fig. 2); weld penetration will refer to the distance δ_H; and the time t_w will be referred to as the seal time. For the data in this paper, the process parameters were varied as follows: hot-tool temperatures from $T_H = 215$ to 395°C; heating times of $t_H = 10$, 15 and 20 s; a melt penetration of $\delta_0 = 0.13$ mm; two weld penetrations of $\delta_H = 0.25$ and 0.66 mm; and a seal time of $t_w = 10$ s.

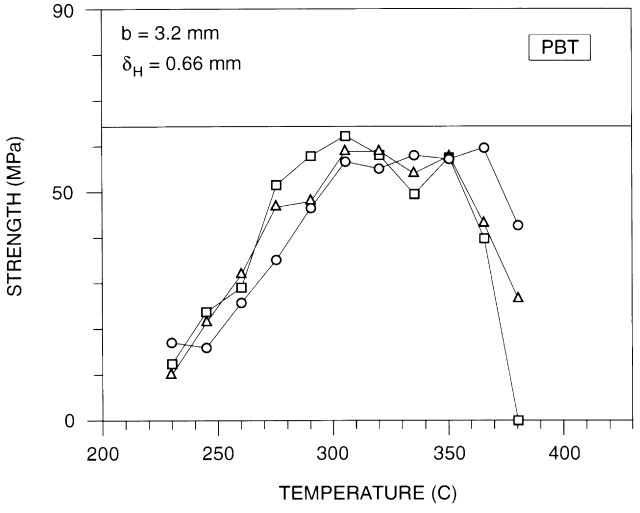

Fig. 14. Weld strength of 3.2-mm-thick PBT as a function of the hot-tool temperature, with the heating time as parameter. Circles, triangles and squares correspond, respectively, to heating times of 10, 15 and 20 s. The melt and weld penetrations were maintained at 0.13 and 0.66 mm, respectively.

5.1. 3.2-mm-thick PBT specimens

Strength and ductility data for 3.2-mm-thick PBT specimens, at a nominal strain rate of 0.01 s^{-1}, as functions of the hot-tool temperature and the heating time, are listed in Table 3. The PBT specimens had a yield strength of 64.8 MPa and a yield strain of 3.64%. The melt penetration was maintained at 0.13 mm, the seal time was kept constant at 10 s, and two weld penetrations of 0.25 and 0.66 mm were used. The first column in this table shows that the hot-tool temperature was varied between 230 and 380°C. The second column shows the three heating times used (10, 15 and 20 s). For a weld penetration of 0.25 mm, columns 3, 5, 7 and 9 list, respectively, the weld strength, the failure strain, the change in length Δl after welding, and the differential penetrations $\Delta\eta$ and $\Delta\eta_T$. Columns 4, 6, 8 and 10 list the corresponding data for a weld penetration of 0.66 mm.

Fig. 13 shows the weld strength (data from Table 3) for a weld penetration of 0.25 mm as a function of the hot-tool temperature for three heating times of 10, 15 and 20 s (indicated, respectively, by circles, triangles and squares). The thin horizontal line represents the strength of the resin (64.8 MPa). For a heating time of $t_H = 10$ s, relative weld strengths (weld strength/strength of PBT resin) lie in the range 0.78–0.87 for hot-tool temperatures in the range $T_H = 275 - 320$°C; the maximum relative strength of 0.87 is obtained at $T_H = 305$°C. The corresponding failure strains are in the range 2.63–4.58%. For $t_H = 15$ s, relative weld strengths ranging from 0.78 to 0.83 are obtained for $T_H = 260 - 305$°C—failure strain are in the range 2.79–3.55%. For $t_H = 20$ s, except for one weld, relative weld strengths of 0.78–0.83 are obtained for $T_H = 260 - 305$°C. Except for one weld, the failure strains for this temperature range vary from 2.74 to 3.36%. Thus, for a weld penetration of 0.25 mm, relative strengths of about 0.80 with fairly high failure strains can be attained over a hot-tool temperature window of 275–305°C.

Fig. 14 shows the weld strength (data from Table 3) for the higher weld penetration of 0.66 mm as a function the hot-tool temperature for three heating times of 10, 15 and 20 s (indicated, respectively, by circles, triangles and squares). For a heating time of $t_H = 10$ s, relative weld strengths of 0.88–0.90 can be obtained in the hot-tool temperature range $T_H = 305 - 350$°C, and a maximum relative strength of 0.92 is obtained at $T_H = 365$°C. The corresponding failure strains are in the range 2.69–3.74%. For $t_H = 15$ s, relative weld strengths of about 0.90 are obtained for $T_H = 290 - 350$°C—failure strain are in the range 3.15–4.27%, except one at 2.83%. For $t_H = 20$ s, relative weld strengths of about 0.90 are obtained for

Table 4
Comparison of the strength and ductility data for hot-tool welds of 3.2- and 6.1-mm-thick PBT specimens, at a strain rate of $\dot{\varepsilon} = 0.01\ s^{-1}$, as functions of the hot-tool temperature and the heating time. The melt and weld penetrations were maintained at 0.13 and 0.66 mm, respectively, and the seal time was kept constant at 10 s

Hot-tool temperature (°C)	Heating time (s)	Weld strength (MPa)		Relative weld strength[a] (%)		Failure strain[b] (%)		Δl (mm)		Differential penetration $\Delta\eta$ ($\Delta\eta_T$) (10^{-2}mm)	
		$b = 3.2$ mm	$b = 6.1$ mm	$b = 3.2$ mm	$b = 6.1$ mm	$b = 3.2$ mm	$b = 6.1$ mm	$b = 3.2$ mm	$b = 6.1$ mm	$b = 3.2$ mm	$b = 6.1$ mm
230	10	17.3[c]	11.8[c]	27	20	0.75	0.43	0.55	0.36	103 (115)	122 (134)
245	10	16.1[c]	29.5[c]	25	49	0.63	1.20	0.83	0.70	75 (89)	88 (102)
260	10	25.6[c]	27.2[c]	40	46	1.05	1.05	1.19	0.93	38 (52)	65 (79)
275	10	35.1	51.0	54	85	1.44	2.25	1.35	1.08	23 (39)	50 (66)
290	10	46.6	51.3	72	86	1.98	2.37	1.56	1.23	1 (17)	34 (50)
305	10	56.8	48.2	88	81	2.69	2.17	1.69	1.46	−11 (5)	11 (27)
320	10	55.4[c]	45.4	86	76	2.93	1.90	1.80	1.64	−23 (−5)	−6 (12)
335	10	58.3	35.4	90	59	3.49	1.37	1.89	1.64	−32 (−14)	−6 (12)
350	10	57.5	58.2	89	97	3.74	4.47	1.84	1.55	−27 (−7)	3 (23)
365	10	59.9	58.7	92	98	3.74	3.56	1.96	1.66	−38 (−18)	−4 (16)
380	10	42.8	40.8	66	68	–	–	2.07	1.83	−50 (−28)	−25 (−3)
395	10	–	27.8	–	46	–	–	–	1.96	–	−38 (−16)
230	15	10.2[c]	16.1[c]	16	27	0.42	0.62	0.64	0.50	94 (108)	108 (122)
245	15	21.5	35.2[c]	33	59	0.83	1.42	1.02	0.77	56 (72)	80 (96)
260	15	32.0	24.2	49	40	1.25	0.95	1.36	1.16	22 (38)	42 (58)
275	15	47.0	44.8	73	75	2.10	1.86	1.49	1.36	9 (27)	22 (40)
290	15	48.1	44.0[c]	74	74	2.12	1.86	1.70	1.51	−13 (7)	6 (26)
305	15	59.1	53.5	91	90	3.15	2.54	1.88	1.64	−30 (−10)	−6 (14)
320	15	59.1	52.0[c]	91	87	3.96	2.42	1.97	1.80	−39 (−17)	−23 (−1)
335	15	54.3[c]	59.0	84	99	2.83	4.15	2.02	1.92	−44 (−22)	−34 (−12)
350	15	58.1[d]	58.3	90	98	4.27	6.98	1.99	1.80	−42 (−18)	−23 (1)
365	15	43.1	50.4	67	84	1.86	2.17	2.02	1.92	−44 (−18)	−34 (−8)
380	15	26.7	24.2	41	41	–	–	2.01	1.89	−43 (−17)	−32 (−6)
395	15	–	18.6[c]	–	31	–	–	–	1.96	–	−38 (−10)
230	20	12.5	22.4	19	38	0.49	0.84	0.70	0.50	88 (104)	100 (116)
245	20	23.6	11.1[c]	36	19	0.98	0.44	1.23	0.93	34 (52)	65 (83)
260	20	29.2	34.4	45	58	1.20	1.44	1.23	1.35	9 (29)	23 (43)
275	20	51.7	50.7	80	85	2.29	2.27	1.78	1.56	−20 (2)	1 (23)
290	20	58.0	49.6	90	83	2.95	2.20	1.87	1.71	−29 (−7)	−14 (8)
305	20	62.5	56.6	96	95	4.59	2.93	1.94	1.82	−37 (−13)	−24 (0)
320	20	58.4	57.7	90	97	3.91	3.00	2.03	1.91	−46 (−20)	−33 (−7)
335	20	49.8	54.5	77	91	2.15	2.54	2.10	1.92	−52 (−26)	−34 (−8)
350	20	57.9	51.6[c]	89	86	3.25	2.34	2.10	1.85	−52 (−24)	−28 (0)
365	20	40.0	31.1	62	52	1.73	1.27	2.01	2.01	−43 (−15)	−43 (−15)
380	20	[e]	20.3	[e]	34	[e]	–	[e]	1.94	[e]	−37 (−7)
395	20	–	17.9[f]	–	30	–	–	–	2.01	–	−43 (−11)

[a] Based on $\sigma_0 = 64.8$ and 59.8 MPa for $b = 3.2$ and 6.1 mm, respectively.
[b] $\varepsilon_0 = 3.64$ and 3.53% for $b = 3.2$ and 6.1 mm, respectively.
[c] Specimen had debris on weld surface.
[d] Specimen yielded below the weld.
[e] Specimen did not weld.
[f] Flash had a greenish hue from residues from copper scraper.

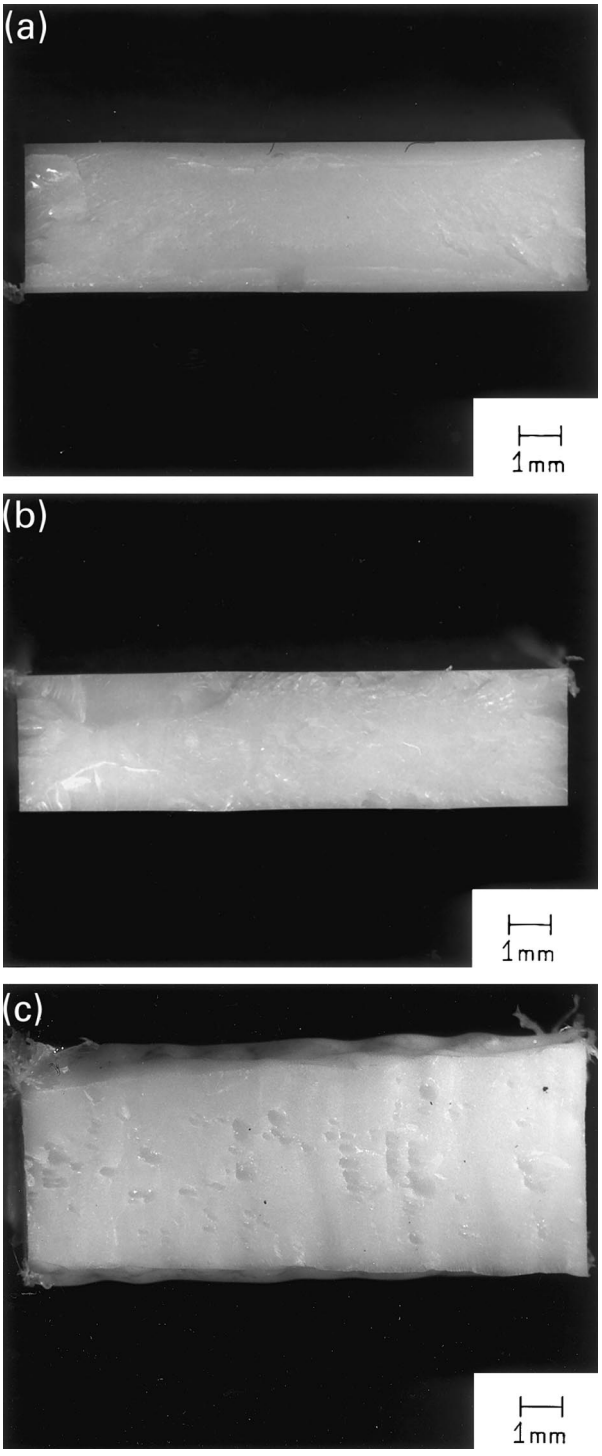

Fig. 15. Fracture surfaces of 3.2-mm-thick PBT specimens for hot-tool welds made at (a) $T_H = 260°C$, (b) $T_H = 320°C$, and (c) $T_H = 380°C$. In these welds, the melt penetration was 0.66 mm and the melt time was 15 s.

$T_H = 305 - 350°C$; in this temperature range, a maximum relative strength of about 0.96 is obtained at $T_H = 305°C$. The failure strains for this temperature range vary from 2.95 to 4.59%. Thus, for a weld penetration of 0.25 mm, relative strengths of about 0.90 with high failure strains can be attained over a hot-tool temperature window of 305–350°C.

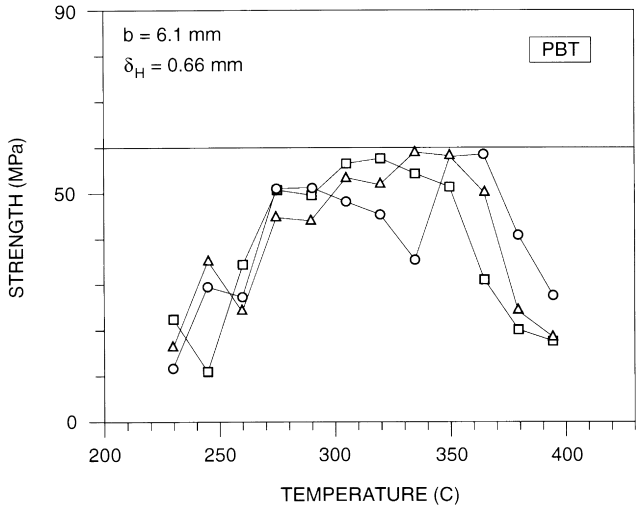

Fig. 16. Weld strength of 6.1-mm-thick PBT as a function of the hot-tool temperature, with the heating time as parameter. Circles, triangles and squares correspond, respectively, to heating times of 10, 15 and 20 s. The melt and weld penetrations were maintained at 0.13 and 0.66 mm, respectively.

The highest weld strengths are obtained at the higher weld penetration of $\eta = 0.66$ mm, for which relative strengths of about 0.9 can be obtained for $T_H = 290 - 350°C$, with a maximum of about $\sigma_R = 0.96$ at $T_H = 305°C$. Over this fairly wide weld process window of $T_H = 290 - 350°C$, the welds exhibit a fair amount of ductility, with failure strains in the range of 2.69–3.74%. For the lower weld penetration of 0.25 mm, the obtainable weld strengths are lower—$\sigma_R = 0.80$ over a hot-tool temperature window of 275–305°C, with a maximum of $\sigma_R = 0.87$ at $T_H = 305°C$.

To correlate variations in weld strength with the weld process conditions, macrographs of the weld fracture surfaces were taken, for $t_H = 15$ s, for three hot-tool temperatures of $T_H = 260$, 320 and 380°C, the weld strength data for which are listed, respectively, in rows 15, 19 and 23 in Table 4. The fracture surfaces for these three cases—for which the relative weld strengths are 49, 91 and 41%, respectively—are shown in Fig. 15a–c, respectively. Fig. 15a, which corresponds to a low $\sigma_R = 49\%$ and a relatively low failure strain of 1.25% (at $T_H = 260°C$), shows most of the fracture occurring in the weld zone. At $T_H = 320°C$, at which the weld has a high relative weld strength of 91% and a high failure strain of 3.96%, the fracture surface includes substantial regions of the specimen away from both sides of the weld zone. At the highest temperature of $T_H = 380°C$, which corresponds to a low relative weld strength of 41%, the fracture surface shows (Fig. 15c) a large number of voids, and the fracture surface is in the weld zone (the added widths of the flash at the top edges makes the specimen look thicker than it is).

Earlier, it was argued that if thermal expansion effects are neglected then the differential penetration $\Delta\eta \geq 0$, and that

stops do and do not contact when $\Delta\eta = 0$ and $\Delta\eta > 0$, respectively. However, when thermal expansion at the heated ends of the specimens is accounted for, a better measure for whether or not stops come into contact is $\Delta\eta_T \geq 0$. The second last column (data for the smaller weld penetration of 0.25 mm) in Table 3 show mostly negative values of $\Delta\eta$, except at the lowest weld temperature of $T_H = 230°C$. Although the corresponding values of $\Delta\eta_T$ are larger, as expected, they are still negative. For the larger weld penetration of 0.66 mm, the last column in Table 4 shows that while $\Delta\eta$ is positive over a wider range of low hot-tool temperatures, it is still negative at higher temperatures. The range of temperatures over which $\Delta\eta$ is positive decreases with increases in heating time. $\Delta\eta_T$ is positive essentially over the same temperature range.

One explanation for this discrepancy would be errors in the measurements of δ_0 and the weld penetration δ_H. Instead of the two stops shown in the schematic in Fig. 2, contact is actually determined by four stops on each side. The difficulty in establishing even contact among the four stops on each side could result in errors in δ_0 and δ_H. A combined small increase of $\delta = \delta_0 + \delta_H = 0.25$ mm would make all values of $\Delta\eta_T$ greater than or equal to zero. This argument is supported by the fact that, for the same process conditions, $\Delta\eta_T$ is mostly larger for the larger weld penetration of 0.66 mm—any systematic error in the measurements would be a smaller fraction of larger settings.

The data in the last two columns of Table 3 do show the following trends that are consistent with expectations based on the underlying physics: first, at any fixed heating time t_H, $\Delta\eta_T$ decreases with increases in the hot-tool temperature T_H. This is to be expected because higher temperatures result in thicker molten layers, thereby allowing for the hot-tool stops to come closer before the melt freezes off. Second, for a fixed hot-tool temperature, $\Delta\eta_T$ again decreases with increases in the melt time; this is explained by increased heating times resulting in thicker molten films.

5.2. 6.1-mm-thick PBT specimens

Strength and ductility data for 6.1-mm-thick specimens are compared with those for 3.2-mm-thick specimens in Table 4, in which columns 4, 6, 8, 10 and 12, list, respectively, the weld strength, the relative weld strength, the failure strain, the change in length Δl after welding, and the differential penetration $\Delta\eta$. In this table, columns 3, 5, 7, 9 and 11 list the corresponding data for 3.2-mm-thick specimens (data from Table 3). The 6.1-mm-thick PBT specimens had a yield strength of 59.8 MPa and a yield strain of 3.53%, both of which are different from the corresponding values (64.8 MPa and 3.64%) for the 3.2-mm thick specimens. Because of the differences between the strengths for the two thicknesses, a comparison of the relative strengths (columns 5 and 6) is more appropriate. The melt penetration was maintained at 0.13 mm, the seal time was kept constant at 10 s, and one weld penetration of 0.66 mm was used. The first column in this table shows that the hot-tool temperature was varied between 230 and 395°C.

Fig. 16 shows the weld strength (data from Table 4) for 6.1-mm-thick specimens for a weld penetration of 0.66 mm as a function of the hot-tool temperature for three heating times of 10, 15 and 20 s (indicated, respectively, by circles,

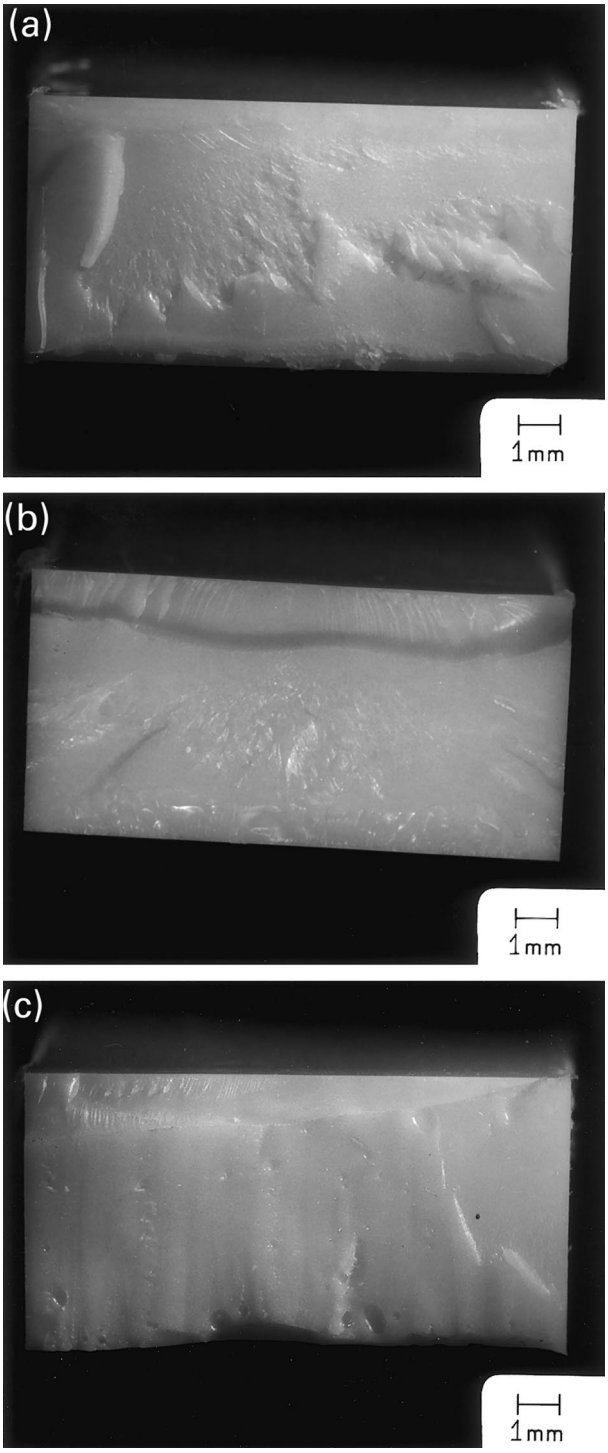

Fig. 17. Fracture surfaces of 6.1-mm-thick PBT specimens for hot-tool welds made at (a) $T_H = 260°C$, (b) $T_H = 335°C$, and (c) $T_H = 380°C$. In these welds, the melt penetration was 0.66 mm and the melt time was 15 s.

Table 5
Strength and ductility data for hot-tool welds of 6.1-mm-thick PBT specimens, at a strain rate of $\dot{\varepsilon} = 0.01\ s^{-1}$, as functions of the hot-tool temperature and the heating time, for a weld penetration of 0.66 mm. The melt penetration was maintained at 0.13 mm, and the seal time was kept constant at 10 s. A set of five specimens were tested at each test condition

Hot-tool temperature (°C)	Heating time (s)	Weld strength[a] (MPa)	Failure strain[b] (%)	Δl (mm)	Differential penetration $\Delta\eta$ ($\Delta\eta_T$) (10^{-2} mm)
320	10	45.4	1.90	1.64	−6 (12)
320	10	35.4	0.51	1.28	30 (48)
320	10	46.5	0.39	1.37	21 (39)
320	10	45.6	2.05	1.39	19 (37)
320	10	25.3	0.94	1.36	22 (40)
335	10	35.4	1.37	1.64	−6 (12)
335	10	56.1	0.54	1.38	20 (38)
335	10	27.7	0.98	1.50	8 (26)
335	10	58.9	3.07	1.48	10 (28)
335	10	51.3	2.58	1.54	4 (22)
350	10	58.2	4.47	1.55	3 (23)
350	10	54.5	2.71	1.48	10 (30)
350	10	58.2	2.86	1.53	5 (25)
350	10	59.6	4.22	1.68	−10 (10)
350	10	53.2	2.37	1.66	−8 (12)
320	15	52.0	2.42	1.80	−22 (0)
320	15	55.8	0.44	1.57	1 (23)
320	15	50.3	0.81	1.54	4 (26)
320	15	58.6	3.07	1.49	9 (31)
320	15	48.6	2.14	1.61	−3 (19)
335	15	59.0	4.15	1.92	−34 (−12)
335	15	60.0	2.25	1.59	−1 (21)
335	15	41.0	2.86	1.60	−2 (20)
335	15	48.0	2.06	1.77	−19 (3)
335	15	61.3	6.10	1.60	−2 (20)
350	15	58.3	6.98	1.80	−22 (2)
350	15	59.5	2.78	1.74	−16 (8)
350	15	60.0	2.27	1.71	−13 (11)
350	15	60.8	6.46	1.76	−18 (6)
350	15	55.5	2.89	1.78	−20 (4)
320	20	57.7	3.00	1.91	−33 (−7)
320	20	40.5	0.68	1.69	−11 (15)
320	20	51.9	2.27	1.71	−13 (13)
320	20	55.6	2.50	1.69	−11 (15)
320	20	58.6	3.32	1.78	−20 (6)
335	20	54.5	2.54	1.92	−34 (−8)
335	20	60.5	2.81	1.80	−22 (4)
335	20	60.7	2.34	1.69	−11 (15)
335	20	57.0	2.87	1.84	−26 (0)
335	20	59.9	6.74	1.65	−7 (19)
350	20	51.6	2.34	1.85	−27 (1)
350	20	56.7	1.90	1.87	−29 (−1)
350	20	51.1	1.59	1.75	−17 (11)
350	20	27.5	1.00	1.85	−27 (1)
350	20	32.8	1.31	1.83	−25 (3)

[a] $\sigma_0 = 59.8$ MPa.
[b] $\varepsilon_0 = 3.53\%$.

triangles and squares). The thin horizontal line represents the strength of the resin (59.8 MPa). For a heating time of $t_H = 10$, with two exceptions at $T_H = 320$ and 335°C, relative weld strengths lie in the range 0.81–0.98 for hot-tool temperatures in the range $T_H = 275 - 365$°C, the highest relative strengths of about 0.98 is obtained in the temperature range of $T_H = 350 - 365$°C. The corresponding failure strains are in the range 2.17–4.47%. For $t_H = 15$ s, relative weld strengths ranging from 0.84 to 0.99 are obtained for $T_H = 305 - 365$°C—failure strain are in the range 2.17–6.98%. For $t_H = 20$ s, relative weld strengths of 0.83–0.97 are obtained for $T_H = 275 - 350$°C. The corresponding failure strains for this temperature range vary from 2.20 to 3.0%.

Table 6
Repeatability of strength and ductility for hot-tool welds of 6.1-mm-thick PBT specimens as functions of the hot-tool temperature and the heating time. The melt and weld penetrations were maintained at 0.13 and 0.66 mm, and the seal time was kept constant at 10 s. The averages and deviations are based on sets of five tests at each test condition (data from Table 5)

Hot-tool temperature (°C)	Heating time (s)	Weld strength[a] (MPa)		Failure strain[b] (%)		Δl (mm)		Differential penetration $\Delta\eta$ ($\Delta\eta_T$) (10^{-2} mm)
		Average	Standard deviation	Average	Standard deviation	Average	Standard deviation	Average
320	10	39.6	9.2	1.16	0.78	1.41	0.14	17 (35)
335	10	45.9	13.6	1.71	1.08	1.51	0.09	7 (25)
350	10	56.7	2.7	3.33	0.95	1.58	0.09	0 (20)
320	15	53.1	4.1	1.78	1.11	1.60	0.12	−2 (20)
335	15	53.9	8.9	3.48	1.68	1.70	0.15	−12 (10)
350	15	58.8	2.1	4.28	2.25	1.76	0.04	−18 (6)
320	20	52.9	7.4	2.35	1.02	1.76	0.09	−18 (8)
335	20	58.5	2.7	3.46	1.85	1.78	0.11	−20 (6)
350	20	43.9	12.9	1.63	0.52	1.83	0.05	−25 (3)

[a] $\sigma_0 = 59.8$MPa.
[b] $\varepsilon_0 = 3.53\%$.

The hot-tool temperatures at which highest weld strengths are obtained in 6.1-mm-thick specimens decrease with increase in heating time: σ_R of about 0.97 for $T_H = 350 - 365$°C for a heating time of $t_H = 10$; $\sigma_R \approx 0.98$ for $T_H = 335 - 350$°C for $t_H = 15$ s; and $\sigma_R \approx 0.96$ for $T_H = 305 - 320$°C for $t_H = 20$ s. The failure strains in these temperature ranges for the three heating times are about 4, 5.5 and 3, respectively. On the basis of these limited tests, the weld process window for obtaining the highest weld strengths with very high failure strains appears to be $T_H = 335 - 350$°C with $t_H = 15$ s. While the temperature ranges for high strengths in 3.2-mm-thick specimens also appears to decrease with increasing heating times ($\sigma_R \approx 0.90$ for $T_H = 335 - 365$°C and $t_H = 10$ s with $\varepsilon_0 \approx 3.7\%$; $\sigma_R \approx 0.91\%$ for $T_H = 305 - 350$°C and $t_H = 15$ s with $\varepsilon_0 \approx 3.6\%$; and $\sigma_R \approx 0.92$ for $T_H = 290 - 320$°C and $t_H = 20$ s with $\varepsilon_0 \approx 3.8\%$), the maximum attainable relative weld strengths are significantly higher in the thicker material.

Macrographs of the weld fracture surfaces, for $t_H = 15$ s, for three hot-tool temperatures of $T_H = 260$, 335, and 380°C—the weld strength data for which are listed, respectively, in rows 15, 20, and 23 in Table 4—are shown, respectively, in Fig. 17a–c. For these three cases, the relative weld strengths are 40, 99 and 41%, respectively. Fig. 17a, which corresponds to a low $\sigma_R = 40\%$ and a relatively low failure strain of 0.95% (at $T_H = 260$°C), shows most of the fracture occurring in the weld zone. At $T_H = 335$°C, at which the weld has a high relative weld strength of 99% and a high failure strain of 4.15%, the fracture surface includes substantial regions of the specimen away from both sides of the weld zone (Fig. 17b). At the highest temperature of $T_H = 380$°C, which corresponds to a low relative weld strength of 41%, the fracture surface shows a large number of voids, and most of the fracture surface is in the weld zone (Fig. 17c).

For 6.1-mm-thick specimens, the last two columns (Table 4) show that, for both weld penetrations, $\Delta\eta$ is positive over a greater temperature range than for 3.2-mm-thick specimens at the same process conditions. And $\Delta\eta_T$ is positive over a larger temperature range; the negative values are less than zero by at most 0.3 mm (0.15 mm for the larger weld penetration). Also, just as for the 3.2-mm-thick specimens, in general, at any fixed heating time t_H, $\Delta\eta_T$ decreases with increases in the hot-tool temperature T_H.

5.2.1. Repeatability of test results

Most of the data in this paper were obtained from one test for each condition. To evaluate the repeatability of weld strength data, sets of five repeat tests were done on 6.1-mm-thick PBT specimens at three hot-tool temperatures (320, 335 and 350°C) and three heating times (10, 15 and 20 s). Weld and melt penetrations of 0.66 and 0.13 mm, respectively, and a seal time of 10 s were used in all these tests. The data for these tests are listed in Table 5.

Mean values and standard deviations for these sets of five

Table 7
Strength and ductility data for hot-tool welds of 3-mm-thick 30-GF-PBT specimens, at a strain rate of $\dot{\varepsilon} = 0.01\ s^{-1}$, as functions of the hot-tool temperature and the heating time, for two weld penetrations of 0.25 and 0.66 mm. The melt penetration was maintained at 0.13 mm, and the seal time was kept constant at 10 s

Hot-tool temperature (°C)	Heating time (s)	Weld strength[a] (MPa)		Failure strain[b] (%)		Δl (mm)		Differential penetration $\Delta\eta$ ($\Delta\eta_T$) (10^{-2} mm)	
		$\delta_H = 0.25$ mm	$\delta_H = 0.66$ mm	$\delta_H = 0.25$ mm	$\delta_H = 0.66$ mm	$\delta_H = 0.25$ mm	$\delta_H = 0.66$ mm	$\delta_H = 0.25$ mm	$\delta_H = 0.66$ mm
215	10	[c]	[c]	[c]	[c]	[c]	[c]	[c]	[c]
230	10	47.1	54.8	0.59	0.71	0.31	0.29	45 (57)	128 (140)
245	10	49.7	55.3[d]	0.63	0.73	0.64	0.61	12 (26)	97 (111)
260	10	50.9	52.8	0.62	0.71	0.90	1.07	−3 (11)	51 (65)
275	10	49.4	50.9	0.64	0.68	0.81	1.32	−5 (11)	25 (41)
290	10	46.2	51.7	0.59	0.66	0.91	1.51	−15 (1)	6 (22)
305	10	52.2	55.5	0.72	0.78	0.86	1.63	−10 (6)	−5 (11)
320	10	48.5	58.0	0.61	0.78	0.93	1.68	−17 (1)	−10 (8)
335	10	42.6	58.0	0.55	0.78	0.96	1.70	−20 (−2)	−13 (5)
350	10	–	51.7	–	0.71	–	1.75	–	−18 (2)
365	10	–	44.7	–	0.63	–	1.75	–	−18 (2)
380	10	–	30.6	–	0.42	–	1.75	–	−18 (4)
215	15	[c]	[c]	[c]	[c]	[c]	[c]	[c]	[c]
230	15	48.5	56.8	0.58	0.73	0.43	0.37	33 (47)	121 (135)
245	15	53.2	56.7	0.70	0.78	0.67	0.89	9 (23)	69 (83)
260	15	48.5	53.1	0.63	0.73	0.82	1.32	−6 (10)	25 (41)
275	15	50.4	53.8	0.63	0.71	0.89	1.54	−13 (5)	4 (22)
290	15	54.9	56.2	0.75	0.76	0.91	1.68	−15 (5)	−10 (10)
305	15	54.4	54.2	0.76	0.76	0.93	1.70	−17 (3)	−13 (7)
320	15	46.7	52.9	0.60	0.76	0.91	1.71	−15 (7)	−14 (8)
335	15	44.6	54.1	–	0.76	0.95	1.77	−19 (3)	−19 (3)
350	15	–	49.3	–	0.66	–	1.71	–	−14 (10)
365	15	–	40.0	–	0.54	–	1.74	–	−17 (9)
380	15	–	24.7	–	0.29	–	1.78	–	−20 (6)
215	20	[c]	[c]	[c]	[c]	[c]	[c]	[c]	[c]
230	20	50.0	56.8	0.63	0.76	0.51	0.43	25 (41)	114 (130)
245	20	51.3	55.4	0.67	0.73	0.75	1.12	1 (19)	46 (64)
260	20	50.1	54.4	0.63	0.76	0.84	1.49	−8 (12)	9 (29)
275	20	50.9	58.1	0.68	0.81	0.91	1.65	−15 (7)	−8 (14)
290	20	51.9	54.8	0.68	0.76	0.90	1.70	−14 (8)	−13 (9)
305	20	48.0	52.5	0.61	0.76	0.97	1.70	−21 (3)	−13 (11)
320	20	50.9	50.5	0.70	0.71	0.93	1.74	−17 (9)	−17 (9)
335	20	41.9	52.8	0.65	0.71	0.93	1.75	−17 (9)	−18 (8)
350	20	–	46.9	–	0.63	–	1.73	–	−15 (13)
365	20	–	28.4	–	0.37	–	1.73	–	−15 (13)
380	20	–	13.9	–	0.17	–	1.79	–	−22 (8)

[a] $\sigma_0 = 112.9$ MPa.
[b] $\varepsilon_0 = 2.74\%$.
[c] Specimen did not weld.
[d] Specimen had debris on weld surface.

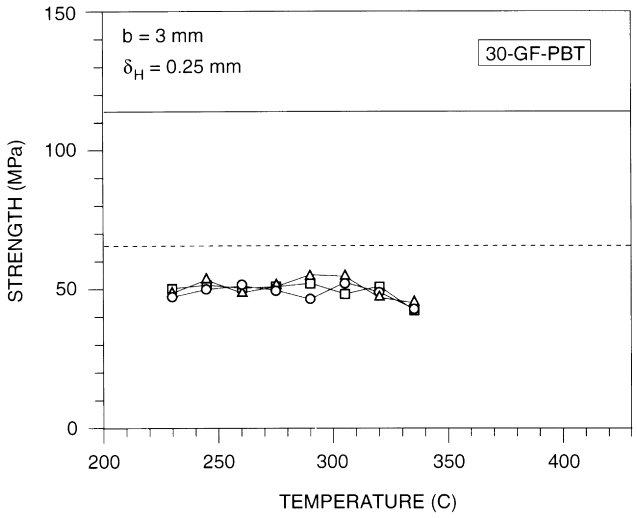

Fig. 18. Weld strength of 3-mm-thick 30-GF-PBT as a function of the hot-tool temperature, with the heating time as parameter. Circles, triangles and squares correspond, respectively, to heating times of 10, 15 and 20 s. The melt and weld penetrations were maintained at 0.13 and 0.25 mm, respectively. The thin horizontal and dashed lines represent, respectively, the mean strengths of 30-GF-PBT (112.9 MPa) and unfilled PBT (64.8 MPa).

repeat tests are listed in Table 6. In descending order, the highest average weld strengths are 58.8 MPa at $T_H = 350°C$ and $t_H = 15$ s; 58.5 MPa at $T_H = 335°C$ and $t_H = 20$ s; and 56.7 MPa at $T_H = 350°C$ and $t_H = 10$ s. The standard deviations in the strengths at these three conditions are less than 5% of the means. Also, the mean failure strains at these three conditions are high (4.28, 3.46 and 3.33%, respectively). Thus, repeatable high weld strength can be expected at these weld conditions. The standard deviations of the strengths at all the other repeat tests in Table 6 vary in the range 8–30%. The standard deviation in length changes is quite small for all the conditions listed in this table.

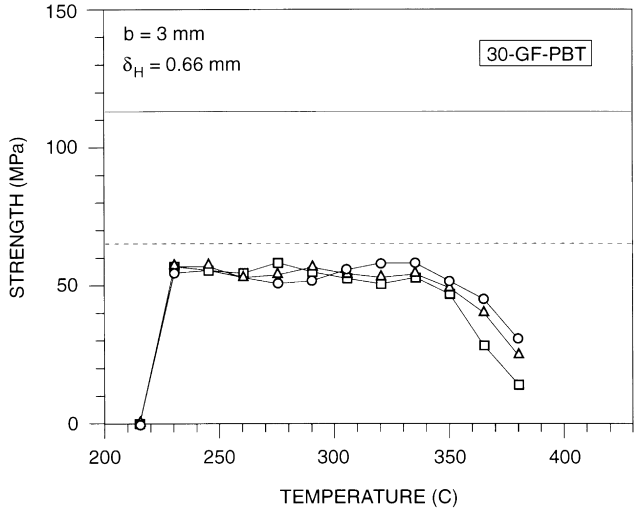

Fig. 19. Weld strength of 3-mm-thick 30-GF-PBT as a function of the hot-tool temperature, with the heating time as parameter. Circles, triangles and squares correspond, respectively, to heating times of 10, 15 and 20 s. The melt and weld penetrations were maintained at 0.13 and 0.66 mm, respectively. The thin horizontal and dashed lines represent, respectively, the strengths of 30-GF-PBT (112.9 MPa) and unfilled PBT (64.8 MPa).

The variations of the weld strength for one test per temperature and heating time are shown in Fig. 16 (data from Table 4). These tests indicated a dip in the weld strength at $T_H = 335°C$ for $t_H = 10$ s, and this weld strength was much lower than for $t_H = 15$ and 20 s. The mean values based on repeat tests (Table 6) do not show this trend—the mean strength at $t_H = 10$ s increases monotonically with the hot-tool temperature. However, for $t_H = 10$ s, of the three test temperatures in Table 6, the largest deviation in strength occurs at $T_H = 335°C$—with a high standard deviation of about 14% of the mean. Also, while the mean weld strength at $T_H = 335°C$ is higher at the other two heating times, it does not occur in the same order as in Fig. 16. The repeat data at $T_H = 350°C$ also have the same trend as in this figure; the strengths are very high and almost equal (with standard deviations less than 5%) at $t_H = 10$ and 15 s, and lower at $t_H = 20$ s (with a high standard deviation of 29%). The trends shown by the mean strengths at $T_H = 320°C$ are similar to those in Fig. 16—lowest strength at $t_H = 10$ s (with a high standard deviation of 23%), but with comparable high strengths at the two greater heating times (with standard deviations of about 8 and 14%, respectively).

While many of the values of $\Delta\eta$ in the last column in Table 5 are negative (by less than 0.35 mm), $\Delta\eta_T$ is mostly positive. The last column in Table 6 that while the average values of $\Delta\eta$ are positive or negative by no more than 0.25 mm, all the average values of $\Delta\eta_T$ are positive.

5.3. Comparison with vibration welds

The vibration welding of a slightly different grade of 6.3-mm-thick PBT (VALOX® 310) is discussed in Ref. [28]. While the reported maximum relative weld strengths, σ_R, are about 0.95, these relative strengths are based on a resin yield strength of 65.2 MPa, while the actual yield strengths of four specimens were 65.2, 61.8, 60.1 and 58.7 MPa [28]. Thus, the static strength of PBT vibration welds can be as high as that of the resin. Clearly, the maximum relative strength of $\sigma_R \approx 0.98$ obtained for hot-tool welds is on the same order as that for vibration welds. Also, the maximum ductilities (strains to failure) of the welds are about the same for the two welding processes.

6. Weld strength of 30-GF-PBT

6.1. 3-mm-thick 30-GF-PBT specimens

Strength and ductility data for 3-mm-thick 30-GF-PBT specimens, at a nominal strain rate of 0.01 s^{-1}, as functions of the hot-tool temperature and the heating time, are listed in Table 7. The 30-GF-PBT specimens had a mean yield

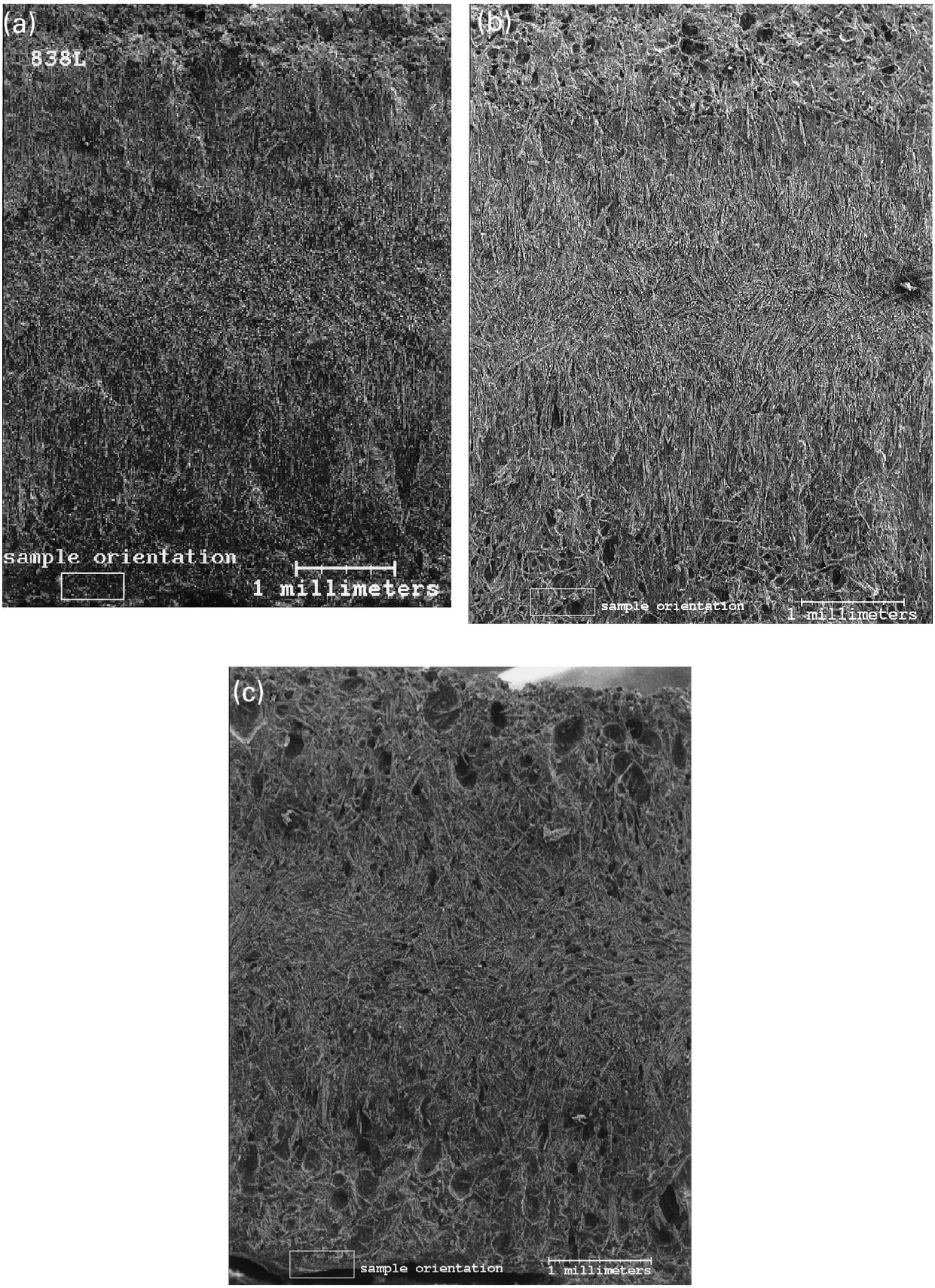

Fig. 20. SEM macrographs of the fracture surfaces of welds showing glass fiber morphology across the thickness of 3-mm-thick specimens, for welds made at (a) $T_H = 260°C$, (b) $T_H = 320°C$, and (c) $T_H = 380°C$. The fibers appear to be randomly oriented in the center, but are aligned in the thickness direction in the outer layers.

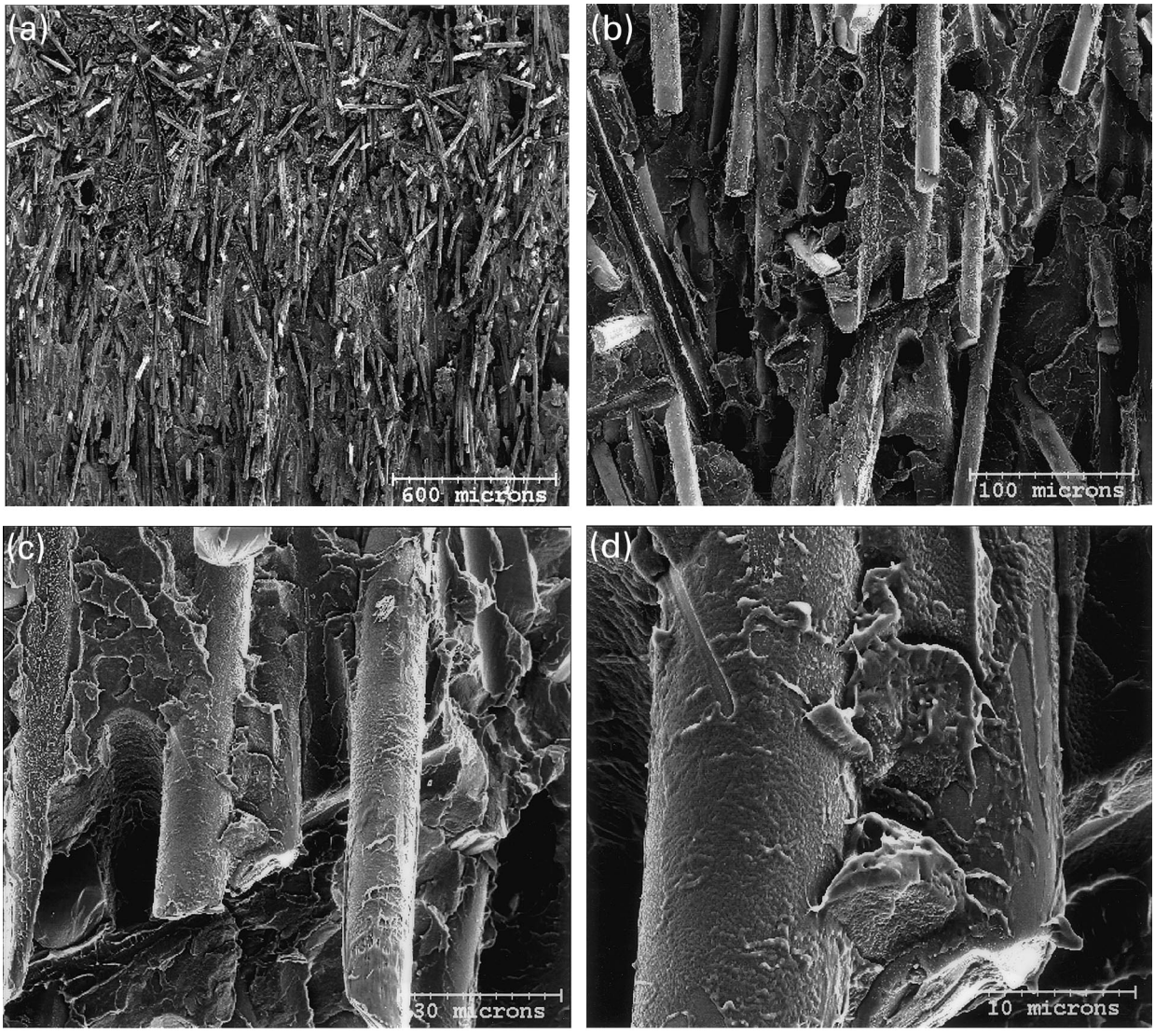

Fig. 21. Higher magnification SEMs of fracture surface of weld made at $T_H = 260°C$. (a) Transition from random orientation at the center to alignment in the cross-thickness direction. (b)–(d) Fibers are well bonded to the resin matrix.

strength of 112.9 MPa and a yield strain of 2.74%—based on tests on four specimens with strengths of 112.4, 111.5, 113.1 and 114.6 MPa and failure strains of 2.98, 2.81, 2.51 and 2.64%. The melt penetration was maintained at 0.13 mm, the seal time was kept constant at 10 s, and two weld penetrations of 0.25 and 0.66 mm were used.

Fig. 18 shows weld strength (data from Table 7) for a weld penetration of 0.25 mm as a function of the hot-tool temperature for three heating times of 10, 15 and 20 s (indicated, respectively, by circles, triangles and squares). The thin horizontal and dashed lines represent, respectively, the mean strengths of the 30-GF-PBT resin (112.9 MPa) and the unfilled PBT resin (64.8 MPa). For a heating time of $t_H =$ 10 s, relative weld strengths lie in the range 0.42–0.46 for hot-tool temperatures in the range $T_H = 230 - 320°C$; the maximum relative strength of 0.46 is obtained at $T_H =$ 305°C. The corresponding failure strains are in the range 0.59–0.72%. For $t_H = 15$ s, relative weld strengths ranging from 0.41 to 0.49 are obtained for $T_H = 230 - 320°C$—failure strains are in the range 0.58–0.76%. For $t_H = 20$ s, relative weld strengths of 0.43–0.46 are obtained for $T_H =$ $230 - 320°C$. The corresponding failure strains for this temperature range vary from 0.61 to 0.70%. Thus, for a weld penetration of 0.25 mm, relative strengths in the range of 0.41–0.49, with failure strains in the range 0.58–0.72%, can be attained over a hot-tool temperature window of 230–320°C.

Fig. 19 shows weld strength (data from Table 7) for the higher weld penetration of 0.66 mm as a function of the hot-tool temperature for three heating times of 10, 15 and 20 s (indicated, respectively, by circles, triangles and squares). For a heating time of $t_H = 10$ s, relative weld strengths of 0.40–0.51 can be obtained over a wide hot-tool temperature range $T_H = 230 - 365°C$, and a maximum relative strength

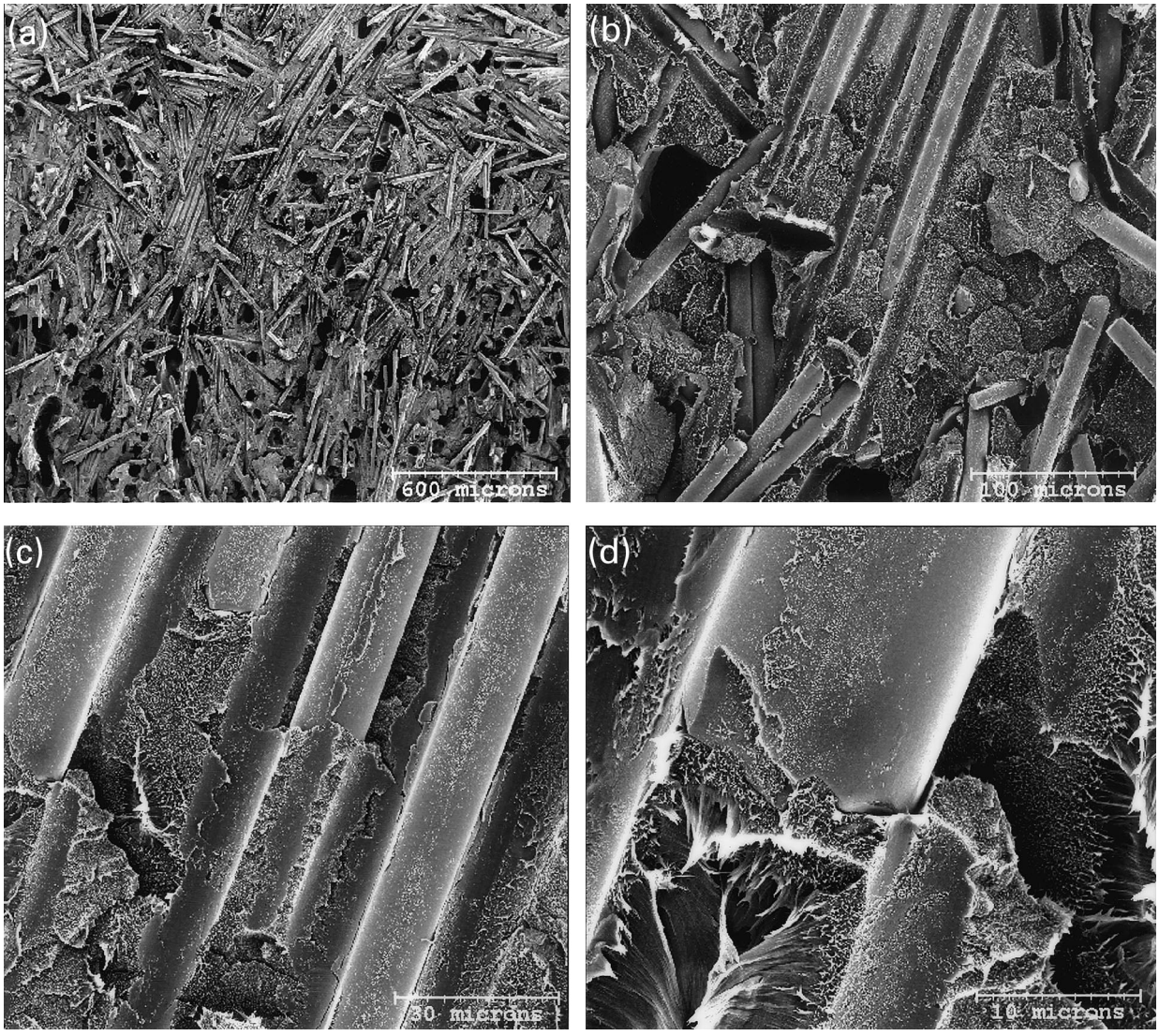

Fig. 22. Higher magnification SEMs of fracture surface of weld made at $T_H = 380°C$. (a) Transition from random orientation at the center to alignment in the cross-thickness direction. (b)–(d) Fibers are not well bonded to the resin matrix. Notice the presence of a large number of voids.

of 0.51 is obtained for $T_H = 335 - 350°C$. The corresponding failure strains are in the range 0.63–0.78%. For $t_H =$ 15 s, high relative weld strengths of 0.47–0.50 are obtained for $T_H = 230 - 335°C$—failure strain are in the range 0.71–0.78%. For $t_H = 20$ s, relative weld strengths of 0.47–0.51 are obtained for $T_H = 230 - 335°C$. The failure strains for this temperature range vary from 0.71 to 0.81%. Thus, for a weld penetration of 0.66 mm, relative strengths in the range of 0.47–0.51, with failure strains in the range 0.71–0.78%, can be attained over a hot-tool temperature window of 230–335°C.

Over the entire temperature range of $T_H = 230 - 380°C$, the weld strengths at the higher weld penetration of $\eta =$ 0.66 mm are consistently higher than those for $\eta =$ 0.25 mm. Also, for the higher penetration, relative strengths in the range of 0.47–0.51 can be obtained over a wide temperature window of $T_H = 230 - 335°C$. The failure strains for the highest strengths range from 0.71 to 0.78. Thus, for this thickness, a maximum weld strength of about $\sigma_R = 0.50$ with failure strains of about 0.75 can be achieved over this fairly wide weld process window.

A comparison of Figs. 18 and 19 (3-mm-thick 30-GF-PBT) with Figs. 13 and 14 (3.2-mm-thick PBT) shows a clear difference between the weldability of the glass-filled and unfilled PBT. In contrast to the glass-filled material, in which the weld strength has a relatively small variation over a wide hot-tool temperature window, the weld strength of the unfilled material is far more sensitive to the hot-tool temperature—the temperature window for high strength is much narrower. Thus, while relative weld strength of the glass-filled material is much lower ($\approx$0.5) than that of the unfilled material ($\approx$1), consistent weld strength can be obtained in the glass-filled material over a much wider weld process window.

Table 8
Comparison of the strength and ductility data for hot-tool welds of 3- and 6.1-mm-thick 30-GF-PBT specimens, at a strain rate of $\dot{\varepsilon} = 0.01\ s^{-1}$, as functions of the hot-tool temperature and the heating time. The melt and weld penetrations were maintained at 0.13 and 0.66 mm, respectively, and the seal time was kept constant at 10 s

Hot-tool temperature (°C)	Heating time (s)	Weld strength (MPa)		Relative weld strength[a] (%)		Failure strain[b] (%)		Δl (mm)		Differential penetration $\Delta\eta$ ($\Delta\eta_T$) (10^{-2} mm)	
		$b = 3$ mm	$b = 6.1$ mm	$b = 3$ mm	$b = 6.1$ mm	$b = 3$ mm	$b = 6.1$ mm	$b = 3$ mm	$b = 6.1$ mm	$b = 3$ mm	$b = 6.1$ mm
215	10	[c]	[c]	[c]	[c]	[c]	[c]	[c]	[c]	[c]	[c]
230	10	51.6	46.9	49	48	0.71	0.85	0.29	0.14	128 (140)	144 (156)
245	10	55.3	48.1	49	49	0.73	0.83	0.61	0.36	97 (111)	122 (136)
260	10	52.8	54.6	47	56	0.71	1.05	1.07	0.51	51 (65)	107 (121)
275	10	50.9	52.1	45	53	0.68	0.85	1.32	0.85	25 (41)	72 (88)
290	10	51.7	50.8	46	52	0.66	0.88	1.51	1.13	6 (22)	44 (60)
305	10	55.5	50.1	49	51	0.78	0.83	1.63	1.32	−5 (11)	25 (41)
320	10	58.0	50.1	51	51	0.78	0.88	1.68	1.55	−10 (8)	3 (21)
335	10	58.0	48.6	51	50	0.78	0.85	1.70	1.56	−13 (5)	1 (19)
350	10	51.7	50.2	46	51[d]	0.71	0.88	1.75	1.65	−18 (2)	−8 (12)
365	10	44.7	52.1	40	53	0.63	0.95	1.75	1.60	−18 (2)	−3 (17)
380	10	30.6	50.6	27	52	0.42	0.88	1.75	1.70	−18 (4)	−13 (9)
215	15	[c]	[c]	[c]	[c]	[c]	[c]	[c]	[c]	[c]	[c]
230	15	56.8	47.6	50	49	0.73	0.81	0.37	0.22	121 (135)	136 (150)
245	15	56.7	48.9	50	50[d]	0.78	0.90	0.89	0.44	69 (85)	113 (129)
260	15	53.1	48.6	47	50	0.73	0.83	1.32	0.83	25 (41)	74 (90)
275	15	53.8	48.9	48	50	0.71	0.85	1.54	1.21	4 (22)	37 (55)
290	15	56.2	49.6	50	51	0.76	0.78	1.68	1.41	−10 (10)	17 (37)
305	15	54.2	50.9	48	52	0.76	0.88	1.70	1.51	−13 (7)	6 (13)
320	15	52.9	53.6	47	55	0.76	0.90	1.71	1.65	−14 (8)	−8 (14)
335	15	54.1	53.6	48	55	0.76	1.00	1.77	1.71	−19 (3)	−14 (8)
350	15	49.3	49.3	44	51	0.66	0.95	1.71	1.68	−14 (10)	−10 (14)
365	15	40.0	44.1	35	45	0.54	0.83	1.74	1.70	−17 (9)	−13 (8)
380	15	24.7	37.7	22	39	0.29	0.66	1.78	1.74	−20 (6)	−17 (9)
215	20	[c]	[c]	[c]	[c]	[c]	[c]	[c]	[c]	[c]	[c]
230	20	56.8	44.4	50	46	0.76	0.76	0.43	0.25	114 (130)	132 (148)
245	20	55.4	51.6	49	53	0.73	0.95	1.12	0.53	46 (64)	104 (122)
260	20	54.4	46.7	48	48	0.76	0.83	1.49	1.05	9 (29)	52 (72)
275	20	58.1	48.9	51	50	0.81	0.78	1.65	1.41	−8 (14)	17 (39)
290	20	54.8	48.7	49	50	0.76	0.83	1.70	1.63	−13 (9)	−5 (17)
305	20	52.5	53.1	47	54[d]	0.76	0.88	1.70	1.66	−13 (11)	−9 (15)
320	20	50.5	49.4	45	51	0.71	0.85	1.74	1.74	−17 (9)	−17 (9)
335	20	52.8	48.9	47	50	0.71	0.93	1.75	1.79	−18 (8)	−22 (4)
350	20	46.9	45.7	42	47	0.63	0.85	1.73	1.80	−15 (13)	−23 (5)
365	20	28.4	39.7	25	41	0.37	0.68	1.73	1.70	−15 (13)	−13(15)
380	20	13.9	10.4	12	11	0.17	0.20	1.79	1.77	−22 (8)	−19 (11)

[a] Based on $\sigma_0 = 112.9$ and 97.6 MPa for $b = 3$ and 6.1 mm, respectively.
[b] $\varepsilon_0 = 27.4$ and 31.5% for $b = 3.2$ and 6.1 mm, respectively.
[c] Specimen did not weld.
[d] Specimen had debris on weld surface.

To correlate variations in weld strength with the weld process conditions, SEMs of the weld fracture surfaces were taken for specimens welded at a weld penetration of $\delta_H = 0.66$, a heating time of $t_H = 10$ s, and three hot-tool temperatures of $T_H = 260$, 320 and 380°C. The weld strength data for these specimens are listed, respectively, in rows 4, 8 and 12 in Table 7; the corresponding weld strengths were 52.8, 58.0 and 30.6 MPa, respectively. The macrographs in Fig. 20a–c show the corresponding morphologies of the glass fibers across the specimen thickness. The most noticeable feature is that while the fibers appear to be randomly oriented in the center, in the outer layers they are aligned in the thickness direction along which squeeze flow occurs during the joining phase. The higher magnification SEM in Fig. 21a, for the specimen welded at $T_H = 260$°C, shows this transition from random orientation to alignment in the cross-thickness direction more clearly. The still higher magnification SEMs in Fig. 21b–d show that in the weld zone the fibers are well bonded to the resin matrix. Higher magnification of the fracture surface of the specimen welded at $T_H = 320$°C are very similar, which is consistent with the relatively high weld strengths at these two weld temperatures. However, at the highest temperature of $T_H = 380$°C, which corresponds to a relatively low weld strength of 30.6 MPa, the fracture surface shows (Fig. 22) a large number of voids and the fibers are no longer well bonded to the matrix. This difference explains the lower weld strength at this high weld temperature.

The last two columns in Table 7 show that $\Delta\eta$ is either positive or is less than zero by at most 0.2 mm. Estimates for the thermally induced expansion δ_T are required for obtaining estimates for $\Delta\eta_T$. Because of paucity of thermal expansion data for glass-filled PBT, estimates for δ_T are not available. The very rough estimates for $\Delta\eta_T$ have been obtained by using estimates for δ_T for PBT. Since glass-filled materials have a lower thermal expansion than the base resin, the positive values of $\Delta\eta_T$ shown may be significantly larger than the actual values.

6.2. 6.1-mm-thick 30-GF-PBT specimens

Strength and ductility data for 6.1-mm-thick specimens are compared with those for 3.2-mm-thick specimens in Table 8, for a weld penetration of 0.66 mm. In this table, columns 4, 6, 8, 10 and 12, list, respectively, the weld strength, the relative weld strength, the failure strain, the change in length Δl after welding and the differential penetration $\Delta\eta$. In this table, columns 3, 5, 7, 9 and 11 list the corresponding data for 3.2-mm-thick specimens (data from Table 7). The 6.1-mm-thick 30-GF-PBT specimens had a yield strength of 97.6 MPa and a yield strain of 3.15%—based on tests on two specimens with strengths of 96.9 and 98.3 MPa and failure strains of 3.17 and 3.12. Again, as with PBT specimens, because the base strengths of the 3- and 6.1-mm-thick 30-GF-PBT specimens are different, relative weld strengths (columns 5 and 6) give a better comparison of weldability. The melt penetration was maintained at 0.13 mm, the seal time was kept constant at 10 s, and one weld penetration 0.66 mm were used.

Fig. 23 shows the weld strength (data from Table 8) for 6.1-mm-thick specimens for a weld penetration of 0.66 mm as a function of the hot-tool temperature for three heating times of 10, 15 and 20 s (indicated, respectively, by circles, triangles and squares). The thin horizontal and dashed lines represent, respectively, the strengths of 30-GF-PBT (97.6 MPa) and unfilled PBT (59.8 MPa). For a heating time of $t_H = 10$ s—with two exceptions at $T_H = 230$ and 245°C, with relative weld strengths of 0.48 and 0.49, respectively—relative weld strengths lie in the range 0.50–0.56 for hot-tool temperatures in the range $T_H = 260 - 380$°C; the highest relative strengths of about 0.56 is obtained at $T_H = 260$°C. The corresponding failure strains are in the range 0.83–1.05%. For $t_H = 15$ s, relative weld strengths in the range 0.50–0.55 are obtained for $T_H = 245 - 350$°C—failure strain are in the range 0.93–1.0%; the strength begins to drop off at higher temperatures. For $t_H = 20$ s, relative weld strengths of 0.50–0.53 are obtained for $T_H = 245 - 335$°C, except for $\sigma_R = 0.48$ at $T_H = 260$°C; the strength drops off at higher temperatures. The corresponding failure strains for this temperature range vary from 0.83 to 0.93%. Thus, by choosing appropriate heating times, relative weld strengths in the range 0.50–0.55 can be achieved over a hot-tool temperature range of $T_H = 230 - 380$°C.

The data in columns 5 and 6 show that the relative weld strengths of the 6.1-mm-thick specimens are higher than, or comparable to, those of the 3-mm-thick specimens over the entire temperature range of $T_H = 230 - 380$°C. Also, the

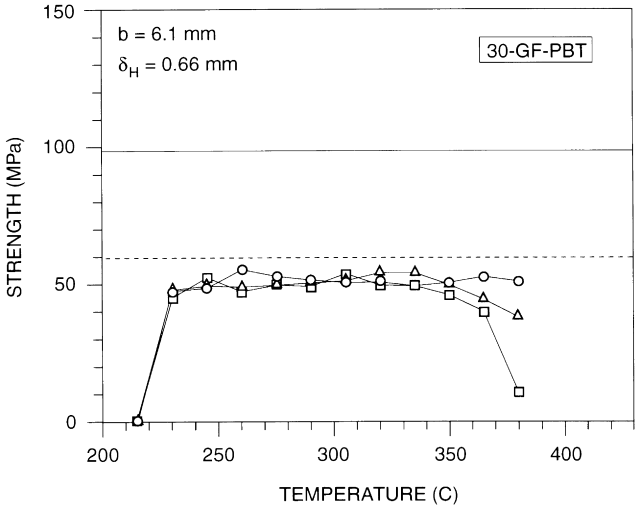

Fig. 23. Weld strength of 6.1-mm-thick 30-GF-PBT as a function of the hot-tool temperature, with the heating time as parameter. Circles, triangles and squares correspond, respectively, to heating times of 10, 15 and 20 s. The melt and weld penetrations were maintained at 0.13 and 0.66 mm, respectively. The thin horizontal and dashed lines represent, respectively, the strengths of 30-GF-PBT (97.6 MPa) and unfilled PBT (59.8 MPa).

maximum relative weld strength (0.56) in the thicker material is larger than that (0.51) in the thinner material. The corresponding failure strain is also higher in the thicker material (1.05 versus 0.81%). Note, however, that because the thinner specimens have a higher tensile strength (112.9 versus 97.6 MPa), higher absolute strengths can be attained in the thinner specimens (58.1 versus 54.6 MPa).

The morphologies of the fracture surfaces of the 6.1-mm-thick specimens are similar to those for the 3-mm-thick specimens. However, as can be seen from the SEM macrograph in Fig. 24—which shows the morphology of the glass fibers across the specimen thickness of a specimen welded at a weld penetration of $\delta_H = 0.66$, a heating time of $t_H = 10$ s, and a hot-tool temperatures of $T_H = 380°C$—the central core with a random glass distribution is much smaller than the outer layers in which the glass fibers are oriented along the thickness direction. Fibers are aligned over a longer distance because the larger specimen thickness results in a longer squeeze flow length. (The weld strength data for this specimen is listed in row 12 in Table 8; the weld strength was 50.6 MPa.) The higher magnification SEM in Fig. 25a shows this transition from random orientation to alignment in the cross-thickness direction more clearly. The still higher magnification SEMs in Fig. 25b–d show that in the weld zone, the fibers are fairly well bonded to the resin matrix—better than for the same process conditions for the 3-mm-thick specimens (Fig. 22); also, the number of voids is much smaller. Micrographs for 6.1-mm-thick specimens welded at $T_H = 320$ and 260°C (rows 8 and 4, respectively in Table 8) are very similar to those for $T_H = 380°C$, except that the fibers bond better to the matrix at lower temperatures and there are progressively smaller number of voids. This is consistent with the relatively high weld strengths of 50.1 and 54.6 MPa, respectively, at these two weld temperatures.

The discussion on values of $\Delta\eta$ and $\Delta\eta_T$ shown in the last two columns of Table 8 follows the earlier discussion for these two quantities for the 3-mm-thick glass-filled specimens.

6.3. Comparison with vibration welding

The vibration welding of 30-GF-PBT is discussed in Ref. [26]. Data in Table 6 of that paper show that in 6.1-mm-thick specimens, relative weld strengths of 0.60 and 0.52 can be attained at weld frequencies of 120 and 250 Hz, respectively, the corresponding failure strains being 1.01 and 0.83. Thus, the maximum attainable weld strengths for this material are about the same for hot-tool and vibration welds.

Note that the batch of material used in the vibration welding study [26] was different and the plaques used were molded at a much earlier date. Specimens cut from these plaques had a mean tensile strength of 90.6 MPa and a failure strain of 2.9% (based on a mean over four specimens) as compared to 97.6 MPa and 3.15% for the material used in the present hot-tool welding study.

The relative weld strengths in Table 8 are based on mean strengths of 112.9 MPa (average over four specimens) and 97.6 MPa (mean of two specimens) for the 3- and 6.1-mm-thick specimens, respectively. As already mentioned above, local fiber orientation will have a large effect on the local properties. Thus, a more meaningful relative strength should be based on the local tensile strength, which is difficult to determine. In Ref. [26], a compromise was achieved by calculating a local relative weld strength by dividing the weld strength of a matched pair (Fig. 3) by the tensile strength of a bar cut from the same location. For example, the weld strength of a pair (3, 7) was normalized by the strength of a bar cut from the 3–7 location (Fig. 3). This was a crude attempt to account for fiber orientation effects because the failure location at the weakest point in a tensile bar may not correspond to the fiber orientation at the weld interface. However, a comparison of the two types of relative weld strength (Table 6 in Ref. [20]) does give an indication of the amount of scatter that may be expected in weld strength data.

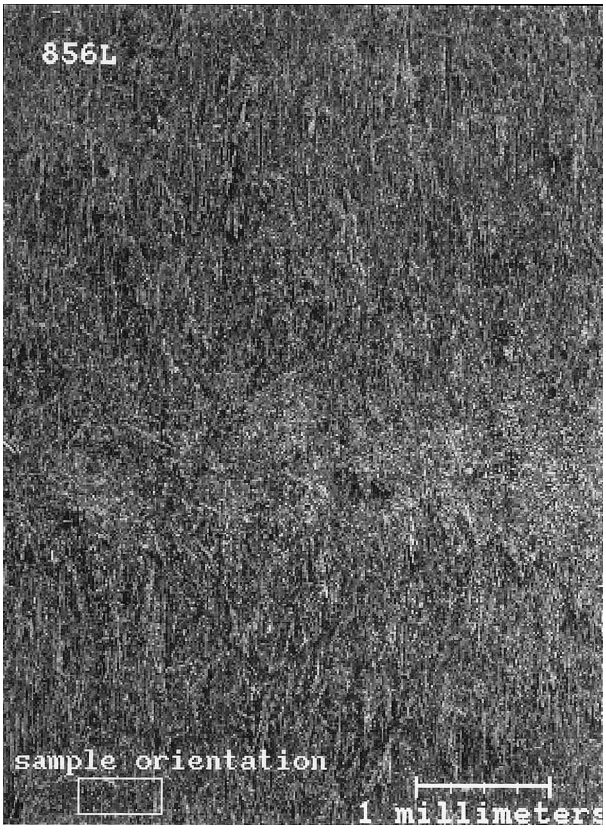

Fig. 24. SEM macrograph of fracture surface of weld showing the glass fiber morphology across the thickness of a 6.1-mm-thick specimen welded at $T_H = 380°C$. In comparison to 3-mm-thick specimens (Fig. 20), the central core of randomly oriented fibers in the 6.1-mm-thick specimen is relatively much smaller than the thickness of the outer layers in which the fibers are aligned along the thickness direction.

7. Concluding remarks

It has been shown that high strengths can be attained in hot-tool welds of PBT specimens. Relative weld strengths in excess of 90% have been demonstrated for $T_H = 290 - 350$°C, with a maximum of about 96% at $T_H = 305$°C. In the 6.1-mm-thick material, higher relative weld strengths of about 99% have been demonstrated for temperatures in the range $T_H = 305 - 365$°C. The thickness of the part does have a small effect—with increasing part thickness, the optimum temperature process window appears to shift to higher temperatures. A higher weld penetration appears to result in higher weld strength. An increase in the heating time appears to reduce the hot-tool temperature required for obtaining high weld strengths. These hot-tool weld strengths compare very favorably with vibration welds for this material.

In glass-filled materials, relative weld strengths of about 50% can be obtained in the 3-mm-thick specimens over wide temperatures in the range $T_H = 230 - 380$°C. In the 6.1-mm-thick material, the relative strengths are consistently higher than for the thinner specimens; a maximum weld strength of about 55% has been demonstrated. However, because the thinner specimens have a higher tensile strength, higher absolute strengths can be attained in the thinner specimens. The hot-tool weld strengths of these glass-filled materials also compare favorably with vibration welds.

Most of the data in this paper were obtained from one test per weld process condition studied. While such data do not provide information on repeatability, they are useful for an initial mapping of weldability over a wide range of weld process conditions. Repeatability studies show that high average weld strengths can be achieved in 6.1-mm-thick specimens—the highest average weld strengths obtained

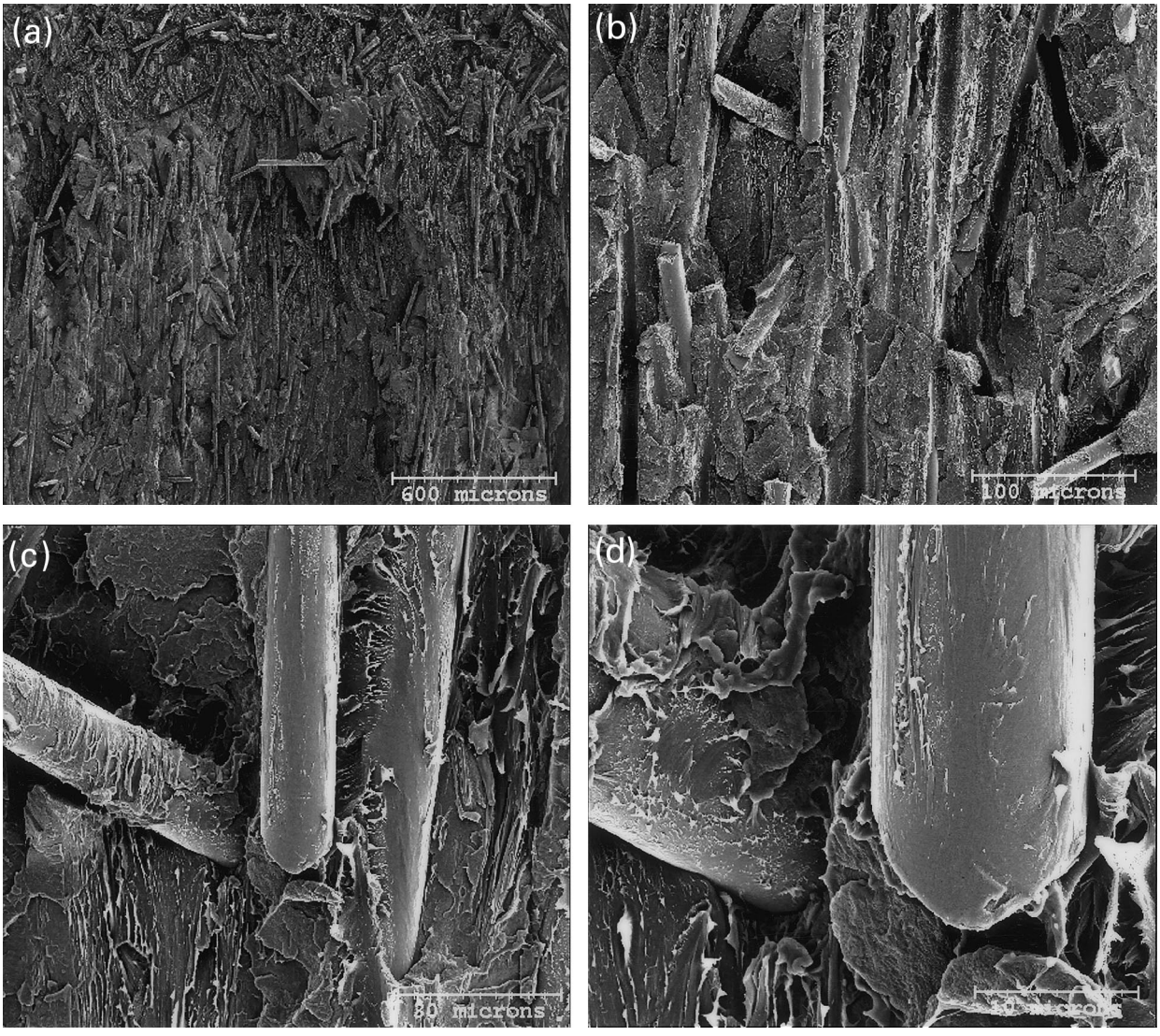

Fig. 25. Higher magnification SEMs of fracture surface of a 6.1-mm-thick specimen welded at $T_H = 380$°C. (a) Transition from random orientation at the center to alignment in the cross-thickness direction. (b)–(d) Fibers are relatively well bonded to the resin matrix.

were 58.8 MPa at $T_H = 350°C$, 58.5 MPa at $T_H = 335°C$, and 56.7 MPa at $T_H = 350°C$, with the standard deviations being less than 5%. While hot-tool welding can produce strong welds, it requires careful dimensional and hot-tool temperature control, and a continuous cleaning of the hot-tool surface. In contrast, it is much easier to control the weld processing conditions in the vibration welding process.

Careful measurements of the differences between the initial and final lengths of specimens have not completely been reconciled with the differences expected on the basis of the machine stop settings. This discrepancy may either result from inaccuracies in the machine or from an inadequate analysis of thermal expansion effects. The length change data in this paper provide information for a more careful analysis of this welding process. The apparent variability of this welding process points to the need for more data at each test condition for a better mapping of the optimum welding conditions.

Acknowledgements

This work was supported by GE Plastics and the NIST ATP project: Engineering Design with Injection-Molded Thermoplastics. The contributions of K.R. Conway, who carried out all the tests, and the inputs of L.P. Inzinna are greatly appreciated.

References

[1] Stokes VK. Polymer 1999;40:6235.
[2] Stokes VK. Polym Eng Sci 1989;29:1310.
[3] Potente H, Natrop J. Polym Eng Sci 1989;29:1649.
[4] Barber P, Atkinson JR. J Mater Sci 1972;7:1131.
[5] Barber P, Atkinson JR. J Mater Sci 1974;9:1456.
[6] Bucknall CB, Drinkwater IC, Smith GR. Polym Eng Sci 1980;20:432.
[7] Egen U, Ehrenstein GW. DVS Berichte 1983;84:49.
[8] Andrews JRF, Bevis M. J Mater Sci 1984;19:645.
[9] Andrews JRF, Bevis M. J Mater Sci 1984;19:653.
[10] Watson MN, Murch MG. Polym Eng Sci 1989;29:1382.
[11] Gehde M, Bevan L, Ehrenstein GW. Polym Eng Sci 1992;32:586.
[12] Bowman J, Haunton J, Folkes MJ. SPE ANTEC Tech Papers 1990;36:1793.
[13] Nonhof CJ. Polym Eng Sci 1996;36:1184.
[14] Potente H. Kunststoffe 1977;67:17.
[15] Potente H. DVS Berichte 1983;84:41.
[16] Potente H, Tappe P. Polym Eng Sci 1989;29:1642.
[17] Pimputkar SM. Polym Eng Sci 1989;29:1387.
[18] Poslinski AJ, Stokes VK. Polym Eng Sci 1992;32:1147.
[19] Poslinski AJ, Stokes VK. SPE ANTEC Tech Papers 1992;38:1228.
[20] Gabler K, Potente H. J Adhesion 1980;11:145.
[21] Potente H, Gabler K. Plastverarbiter 1980;31:203.
[22] El Barbari N, Michel J, Menges G. Kunststoffe 1986;76:20.
[23] El Barbari N, Michel J, Menges G. Kunststoffberater 1986;31:63.
[24] Muschik H, Radax M, Dragaun H, Eichinger F. Kunststoffe 1986;76:23.
[25] Stokes VK. Polymer 1998;39:2469.
[26] Stokes VK. Polymer 1993;34:4445.
[27] Stokes VK. Polym Eng Sci 1997;37:692.
[28] Stokes VK. Polym Eng Sci 1988;28:998.